A FUNDAMENTAL STUDY OF SPARK IGNITION FOR A LARGE-BORE SINGLE CYLINDER NATURAL GAS ENGINE

A Thesis

by

FORREST G. POMMIER

Submitted to the Office of Graduate and Professional Studies of
Texas A&M University
in partial fulfillment of the requirements for the degree of

MASTER OF SCIENCE

Chair of Committee,	Timothy Jacobs
Committee Members,	Jerald Caton
	Sergio Capareda
Head of Department,	Andreas Polycarpou

May 2020

Major Subject: Mechanical Engineering

ABSTRACT

The natural gas industry has entered a substantial boom recently as the world seeks out more forms of inexpensive, reliable, and more environmentally friendly energy. Moving this natural gas requires a complex network of pipelines and compressors, including reciprocating engines, to keep the gas moving. These engines are of older design and must be retrofit with modern technologies to improve their performance as well as reduce the emissions that they produce. In this study a directed energy ignition system is tested on a two-stroke, single cylinder engine. Stability and emissions will be observed throughout a range of spark durations and currents for a single speed and load that allows for the most fuel-lean operation of the engine. The results from this study will be analyzed and discussed with Altronic LLC., so as to improve their directed energy ignition technologies.

Many of the pipeline engines in use today lack many of the features found on more modern engines, being as many of the engines are between forty and seventy years old. A challenge under active research by those associated with these engines is in meeting emissions. One means of doing so is by running the engine with less fuel. To accomplish this an ignition system that can send more energy to the spark plug in a controlled manner is of great interest in optimizing for use on these engines. This research investigates a single operating speed and load for 9 different spark energy configurations. Engine operation at these test conditions will allow data of the emissions and engine performance to be assessed in contrast to standard ignition performance.

DEDICATION

To my family

ACKNOWLEDGEMENTS

It is hard to believe to believe that I have been in school for almost six years to study the field of mechanical engineering, and the learning has only just begun. Well before I can remember, my dad would drive me around to watch farmers work the fields and see the amazing equipment used to accomplish the grueling tasks. Traveling to my grandparents' farm and my uncle's landscaping business allowed me to experience the highs and lows of operating and maintaining agricultural and construction equipment. The fascination surrounding how all of those amazing machines planted the seed for my desire to learn everything that I possibly can about engines. I cannot thank my family enough for, unbeknownst to them at the time, introducing me to the world of internal combustion engines.

During my tenure here at Texas A&M University, I was able to have the pleasure of working alongside some fantastic researchers as a member of AERL. Their enthusiasm for engines and desire to help one another when issues arise is one of the greatest assets one could ask for when conducting research. The focus of my experimental work allowed me to work alongside Abdullah Bajwa, Taylor Linker, and Kevin Wallace. Their support in diagnosing issues and enhancing the data collection process were extremely beneficial; this project would not have turned out as it did without their help. My sincere appreciation also extends to Jacob Nowlin, who assisted me in the lab to collect the data, especially during the hot and humid Texas summer days.

The support of my committee members, Prof. Jerald Caton and Prof. Sergio Capareda, are another reason for me to be grateful. These mentors expressed great enthusiasm for my work, shared their time, and were more than accommodating when it came to assisting me as deadlines were approaching.

Finally, it would be considered a crime not to mention my advisor, Dr. Tim Jacobs. His sincere kindness and humbling intelligence were immediately apparent on first meeting him during my initial visit to Texas A&M University. No matter how busy his schedule was during a given day, his willingness to provide assistance on any matter is truly commendable. I thank you, Dr. Jacobs, for this wonderful opportunity to expand my knowledge of the world of IC engines.

CONTRIBUTORS AND FUNDING SOURCES

Contributors

Faculty committee recognition

This research was supervised by a thesis committee consisting Professor Tim Jacobs and Professor Jerald Caton of the Department of Mechanical Engineering and Professor Sergio Capareda of the Department of Biological and Agricultural Engineering.

Student contribution

All research was accomplished independently by the student.

Funding Sources

This work was made possible by Altronic LLC. The spark plug adapter for the capacitor-embedded plug was donated by REAM Corporation.

NOMENCLATURE

AERL	Advanced Engine Research Lab
AFR	Air/Fuel Ratio
AJAX	Ajax E-565
ATDC	After Top Dead Center
BMEP	Brake Mean Effective Pressure
BTE	Brake Thermal Efficiency
BTDC	Before Top Dead Center
CAD	Crank Angle Degree
CD	Capacitive Discharge
CFD	Computational Fluid Dynamics
CO	Carbon Monoxide
CO_2	Carbon Dioxide
COV	Coefficient of Variation
DAQ	Data Acquisition System
DI	Direction Injection
EGT	Exhaust Gas Temperature
F	Fahrenheit
FID	Flame Ionization Detection
HP	Horsepower
IC	Internal Combustion

IMEP	Indicated Mean Effective Pressure
MEXA	Horiba MEXA-7100D; Emissions Analyzer
NDIR	Non-Dispersive Infrared Detection
NI	National Instruments
NOx	Nitrogen Oxides ($NO + NO_2$)
O_2	Oxygen
ppm	Parts Per Million
ppmC	Parts Per Million, Carbon Atom
RPM	Revolutions per Minute
THC	Total Hydrocarbons
UI	User Interface

TABLE OF CONTENTS

Page

LIST OF FIGURES

Page

LIST OF TABLES

Page

1. INTRODUCTION

1.1. The Network of Natural Gas

The natural gas energy sector has continued to be paramount in providing power around the world, with an exceptional increase in recent years in North America. The United States natural gas distribution network is a highly integrated system that moves natural gas throughout the contiguous 48 states and into adjacent markets as well [1]. There are more than 3 million miles of mainline and other pipelines that provide a link from the production regions, such as Marcellus and Eagle Ford, to consumers. In 2018 alone, 28 trillion cubic feet of natural gas was delivered to about 75 million customers throughout the country [2].

In order to move the gas efficiently and safely a large network of pipelines continues to be developed to distribute the energy. Around half of the existing mainline transmission network for natural gas, and a large portion of the local distribution network, were installed in the 1950s and 1960s because consumer demand for more energy more than doubled the demand for natural gas following World War II [2]. The growth of the transmission network in the 21st century began with large growth from 2003 to 2008 when natural gas prices were higher and allowed for development of existing networks and new exploration of natural gas reservoirs. Prices have declined following the economic recession in 2009, which has in turn resulted in an increase in demand for natural gas as a means of electricity generation [2]. As such, new pipelines have continued to be built to link expanded networks and reach new areas around the country, most notably being the Northeast [3].

To transport natural gas many thousands of miles, it is not possible to rely on the pressure of the natural reservoirs alone. Compressor stations are used to assist in the transport through pipelines around the world. These facilities are located every 40-100 miles along a particular pipeline in an aboveground building [4, 1]. The buildings can house either compressors powered by the natural gas from the pipeline or from electricity [5]. A general configuration of a compressor station can be seen in Figure 1.

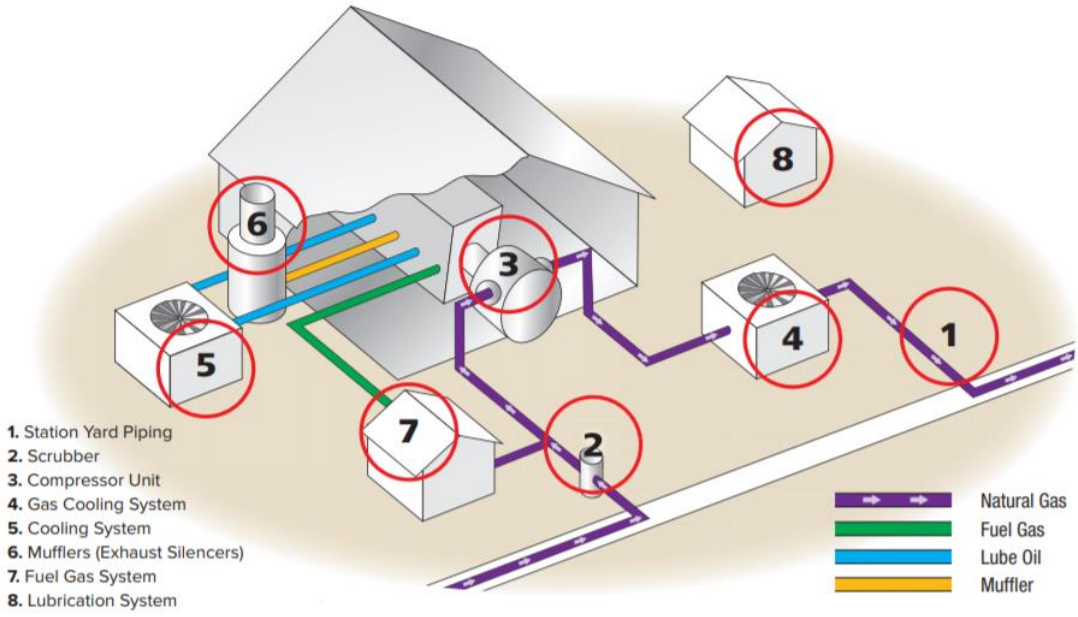

Figure 1. The components of a compressor station [2].

As the gas makes its way through the pipeline and into the compressor station, it begins by going through a scrubber (2) to remove any contaminants they may have been collected in the pipeline. The natural gas is then directed to the compressor unit (3) with some gas siphoned off to fuel the compressor (7). To ensure longevity and efficiency of the compressor unit, a cooling system (5) and lubrication system (8) are used in

conjunction. Then, as the gas exits the compressor unit it is now at a higher pressure and also a higher temperature. The natural gas passes through a cooling system (4) before returning to the main pipeline and continuing on to its destination.

Compressor stations can house three different types of engines to provide power to the compressors, known as prime movers. A turbine uses natural gas to power the rotating radial compressor blades, similar to a large fan that increases the pressure of the gas in the pipeline [6]. An electric motor is similar to the turbine in that is uses radial compressors, though it requires a reliable high-voltage power source in order to operate. Reciprocating engines are the final means of compressing the natural gas and act in a similar means to an automobile engine, though on a much larger scale. The engines use natural gas to fuel the power pistons in the compressor engines [7]. Attached to the same crankshaft as the power pistons are the compressor pistons located in cylinder cases on the side of the engines [8]. These pistons are used to compress the natural gas and send it on its way through the pipeline. The major advantages of reciprocating compressors are that: the volume of gas being pushed through the pipelines can be adjusted incrementally to meet changes in demand and the compressors stations are also extremely reliable, as many engines have been in services for decades [5, 8].

1.2. Two-Stroke Engine Operation

1.2.1. The Two-Stroke Cycle

The compressor engines used to assist in moving natural gas along a pipeline can be either a four-stroke or two-stroke variant. The engine used for this study is of two-stroke design, so that will be the focus here. Two-stroke engines have a higher power

output for a given engine size that their counterpart, the four-stroke, given that a power stroke takes place every revolution instead of every 2 revolutions [9, 10]. The two-stroke engine design is also simpler in nature with all processes controlled at the upper and lower edges of the piston as it transitions up and down within the cylinder. Starting the cycle with the piston at TDC, the air and fuel mixture between the piston crown and cylinder head is ignited by the spark plug as shown in Figure 2 of an AJAX single-cylinder engine.

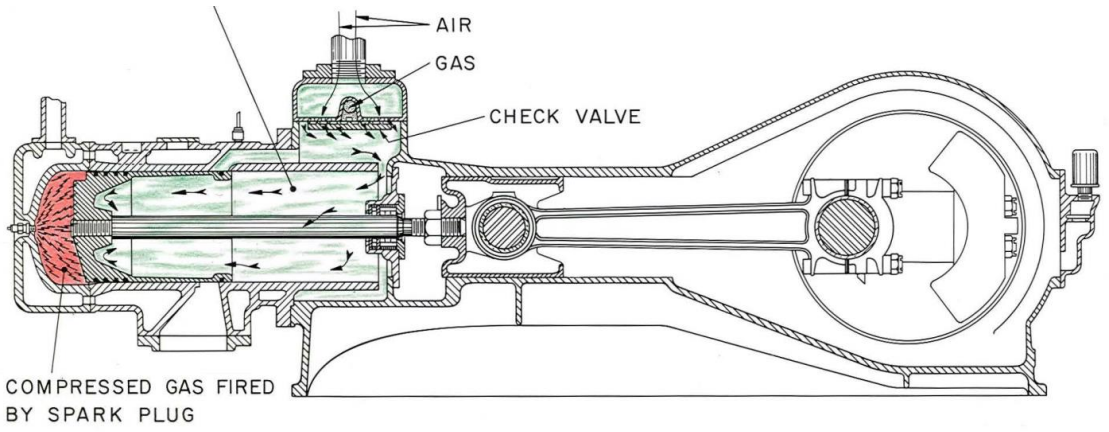

Figure 2. The beginning of the expansion of the expansion stroke [11].

This ignition of the mixture initiates a rapid increase in temperature and pressure causing the gasses to expand, thus driving the piston downward. At the same time that the piston is at TDC and combustion is starting, fresh air is admitted through the intake port from atmosphere to the crank case. This is due to the increasing volume lowering the pressure in the crank case below that of the volume containing the fresh air. Fuel admittance can be accomplished either by means of carburation when the intake port is open or by direct fuel injection to the cylinder after the exhaust ports have closed [10].

Above the piston, as combustion ends, the piston slides downward past the exhaust ports, which is called the release point in the cycle. This point allows the exhaust gasses to exit the cylinder in a pulse of hot, high-pressure gas. As the area of the exhaust port increases with crankshaft angle, the cylinder pressure is simultaneously decreasing. The exhaust pressure profile increases to a maximum and then decreases with time. This flow process is considered unsteady and such a pulse can have a dramatic impact on the performance of the engine [10, 9]. The initial exhaust process, known as blowdown, ends as the piston continues towards BDC and the intake or transfer ports open, thus starting the scavenging process shown in Figure 3.

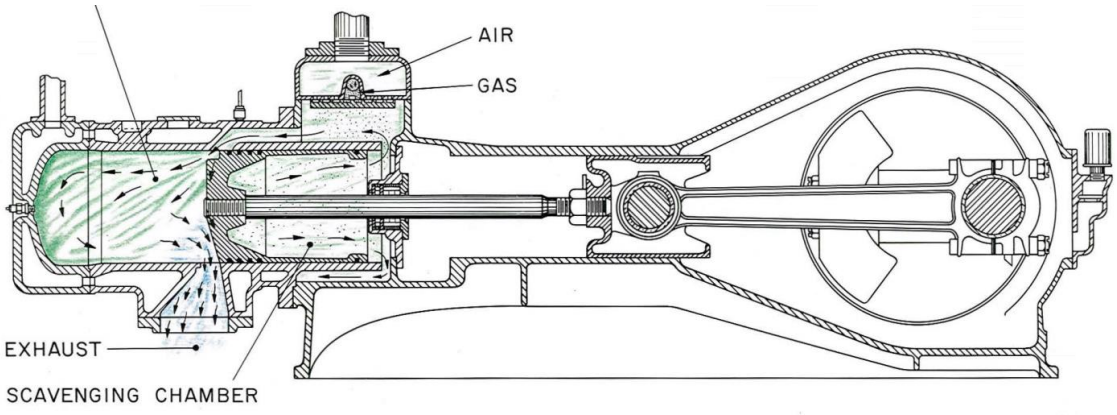

Figure 3. The scavenging process during expansion [11].

During scavenging, the pressure of the fresh air and fuel in these ports is higher than that in the cylinder allowing the mixture to rush into the cylinder. Poor port design will cause the fresh mixture to exit the exhaust port instead of staying within the cylinder to take part in the next cycle's combustion process [12]. This loss of fresh mixture to the exhaust port is called short circuiting. The degree of short circuiting in a two-stroke can

have a dramatic effect on the next combustion event and result in less pressure rise and power output. Additionally, a large portion of the fuel in a pre-mixed configuration would exhaust to the atmosphere and result in an enormous emittance of unburned hydrocarbons. Hence, the guidance of the fresh air-fuel mixture into the cylinder, from the transfer ports should be designed to ensure maximum retention within the cylinder [10]. Reaching the trapping point, when the exhaust port is completely closed, the scavenging process has been completed, as displayed in Figure 4.

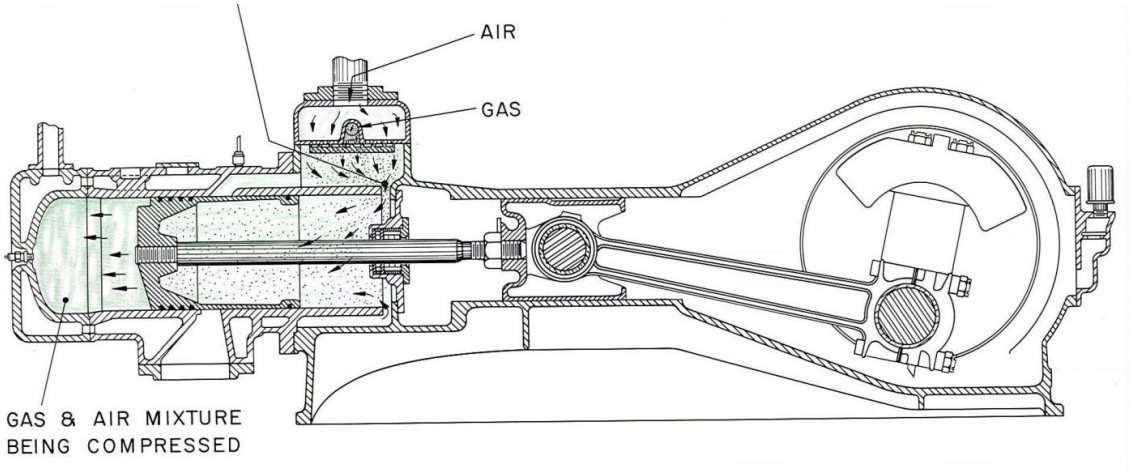

Figure 4. The new trapped mass being prepared for combustion [11].

The cylinder is now filled with a combination of fresh air, and fuel if pre-mixed, along with some exhaust gasses from the previous combustion cycle that did not get exhausted. As the exhaust port is closing the pressure continues to rise, while also spilling some of the fresh mixture into the exhaust port. Upon complete closing of the exhaust port, the compression process truly begins, continuing until the piston reaches TDC. The beginning of combustion in a spark-ignited engine depends on when the spark

plug is activated. The timing of the spark event will dictate when the peak pressure will occur in the compression or expansion process [10, 13].

1.2.2. Scavenging Processes

Scavenging is a major disadvantage for the two-stroke engine because it allows fresh fuel and air mixture to be lost by exiting the exhaust port while gases from the previous combustion event are also exiting the cylinder [9]. The piston in the engine, as well as the ports, are designed to guide the incoming fresh charge away from the exhaust port. The variation in these designs have allowed for the development of different types of scavenging. In order for scavenging to be efficient, the incoming fresh charge must be at a high enough pressure to displace the exhaust gases remaining in the cylinder. The increase in pressure is done so either by the expansion stroke of the cylinder (natural aspiration) or by a separate turbocharger (utilize exhaust gasses) or blower (mechanically driven) [9, 12]. Scavenging can be accomplished in a variety of methods including: loop, cross, and uni-flow scavenging. How these are defined depends on the location of the ports and/or valves and how the components direct the fluid movement within the cylinder [13].

The loop and cross scavenging use only ports in the cylinder walls to exhaust and bring in air and fuel [9]. These are certainly the most common types of scavenging as they have a greater reliability than the movement of valves. The key difference between the two scavenging methods is that cross scavenging has the exhaust and intake ports on opposite sides of the cylinder. Uni-flow scavenging uses a combination of ports and valves to accomplish its operation [12]. The ports are used to provide a fresh charge to

the cylinder and subsequently push the remaining combustion products through the previously opened exhaust valves, in most cases. Some engines use the valves and ports for the opposite functions [12].

Even though the geometries could vary greatly between the scavenging methods the general process is the same—get rid of as much exhaust gas as possible while retaining and thoroughly mixing the fresh charge. Ultimately, it has been shown that the more efficient method of scavenging, meaning less mixing of the exhaust and intake gases, is by increasing the number of intake ports while also reducing their physical size [13, 12]. Fundamentally this means that more of the gasses are be guided by boundaries of the ports than by adjacent fluid molecules found on engines with larger and fewer ports and valves.

1.2.3. Gas Control Strategies

The simplest method of gas transfer in an engine is by movement of a piston exposing and closing off ports. This means that the timing of all events is symmetrical with respect to TDC. The most popular means of asymmetrical inlet and exhaust timing is by the use of disc valves, reed valves, and poppet valves. Asymmetrical timing permits phasing of the ports to have a better correspondence with the pressure event in the cylinder, or the crankcase, and provides more control to optimize the exhaust or intake gas flow [10].

Disc valves have timing characteristics that require some shaft on which to provide timing for the engine, which then becomes very complex for multi-cylinder engines. This design was initially designed for racing motorcycles in the 1950s, but have

been supplanted by the reed valve design [10]. Reed valves have always been a popular design choice for outboard motors, as they provide an effective automatic valve whose timing varies with both engine load and speed. The reed is actuated by the pressure differential between the intake port and the engine cylinders, resulting in a fluttering motion, like a hummingbird, during operation [10, 12]. Most reed valves are designed with the reed petals being spring steel or a fiber-reinforced composite material. The composite material is mainly desired for high-speed racing engines [10]. Poppet valves are difficult to implement on a two-stroke engine so as to provide adequate charge into the cylinder. Meaning, the valves cannot be opened and closed at the appropriate times during operation, especially at higher engine speeds. It should also be noted that the timing of the intake and exhaust process for a two-stroke is about half that of a four-stroke engine, where poppet valves are the standard [10].

In more recent decades as emissions have become a greater priority to reduce, the means of fuel admission into the cylinder has changed. Many engines today have switched from a homogeneous mixture entering the cylinder through the ports, to strictly air entering from the ports. This substantially improves the scavenging of the engine by completely eliminating short-circuiting in the engine. The engine, instead, receives fuel from a system the directly injection fuel into the cylinder once the exhaust ports have closed on the engine. An increase in control over the engine parameters is also achieved by having a new means of timing, which is asymmetrical, similar to that discussed with the various valve configurations.

1.3. Spark Ignition Systems

1.3.1. Creating the Spark

To initiate combustion in a spark ignition engine, a spark plug is used to create an electrical discharge that ignites the air-fuel mixture near the end of the compression stroke [9]. In order for this combustion process to occur, all of the required components must be present. This includes fuel and air being mixed to the correct mass ratio within the spark plug gap and optimal flow velocity when the spark occurs [14]. The spark itself is made up of: the pre-breakdown phase, the breakdown phase, the arc phase, and finally the glow phase. A summary of the timing for all of the spark phases can be seen below in Figure 5.

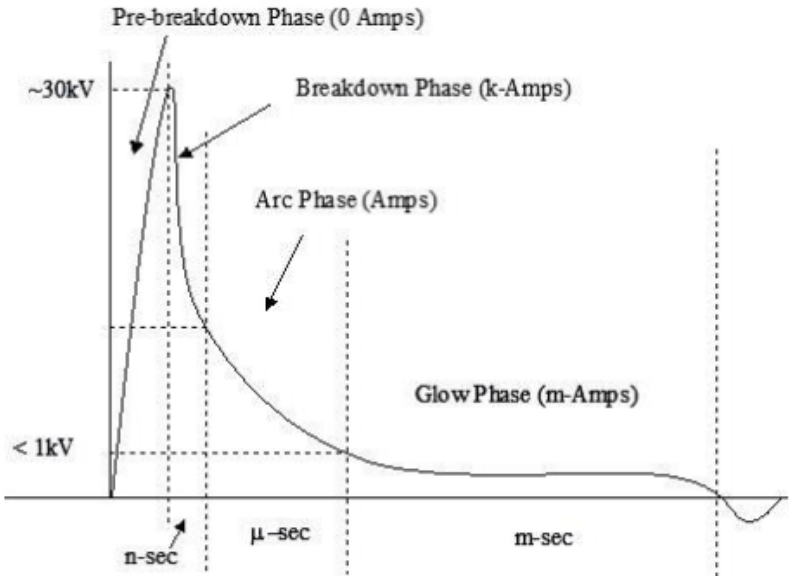

Figure 5. Voltage and duration of each spark phase [15].

During the pre-breakdown phase the voltage potential across spark plug gap is increasing, causing electrons to accelerate towards the center electrode. Within a sufficiently high electric field, the electrons can ionize the molecules they collide with leading to the second phase known as breakdown [13, 16]. The breakdown phase begins with an over-exponential increase in current with values reach several hundred amps within about 10 nanoseconds, meaning that many positive ions are colliding against the cathode at high speeds [9]. Simultaneously, a decrease then occurs in the potential difference and electric field across the spark plug gap [13]. Maly suggests the minimum energy required to initiate the breakdown at ambient conditions is about 0.3 mJ. This breakdown causes a rapid increase in temperature and pressure with maximum values reaching 60,000 K and several hundred bar [16]. These extremely high pressures result in intense shock waves as the spark channel expands at supersonic speed. The expansion of the channel allows the conversion of potential energy to thermal energy and facilitates cooling of the plasma. It is during this phase that pools of molten material that make up the cathode are formed due to this relentless impact by the positive ions. The anode also develops a pool of material due to recombination of the electrons. The end of the breakdown phase occurs upon the development of a hot spot on the cathode, which turns the discharge into an arc [15].

The arc phase produces a much lower voltage and a current as high as the ignition system allows, for a relatively longer period of time than during the breakdown phase [13, 15]. The arc discharge is sustained by electrons emitted from the cathode hot spots. This process can result in damage of the electrodes because of the relatively

higher electrical power being transferred to the electrode surfaces, with the erosion rate increasing with the plug gap. For a typical ignition system, the burning voltage is about 100 volts and the current is greater than 100 mA. It is during this phase when heat losses become substantial as it is transferred to the electrodes. The heat losses due to radiation throughout the spark event have been determined to be inconsequential [15]. The heat losses increase with increased energy supplied to the spark plug, meaning that mixtures that are either rich or lean result in a less efficient spark discharge [16]. Depending on the conditions both in the cylinder and of the ignition system, the efficiency of the energy-transfer from the arc discharge to thermal energy of the air-fuel mixture is between 10 and 50 percent [13].

Once the so-called ‘pathway’ as been established across the gap, the glow discharge phase begins. This phase depends on the ignition systems components, but it essentially describes the action of the energy storage device releasing its energy into the circuit to be sent through the spark plug [9]. In the glow phase the current and voltage follow the trend of being lower than the preceding phase with a much longer duration [16]. Currents of less than 100 mA results in the arc discharge phase becoming a glow discharge. Electrons are freed by impacts of ions during this phase; a less efficient process than thermionic emission for an arc discharge. Glow discharges are more common in practice as they result in lower erosion rates, though arc discharges are inherently more efficient in energy transfer [13]. Also, if the current sent during the glow discharge phase is too much, then heavy electrode erosion will occur and reduce the effectiveness of the spark plug [9]. Nevertheless, the electrode damage can be minimized

by arc travel with sufficient flow between the spark plug gap. Arc travel is the movement of the arc that expands the pathway between the electrodes and creates the shape of a bow. In the case of low flow conditions where the arc is stationary, the amount of power transferred to the surfaces can be extremely high and therefore increase the amount of damage that had already be created on the electrode surfaces by the previous two phases. However, with relatively high flow this is not an issue as sufficient arc travel can be achieved, which reduces the damage caused to the surfaces by transferring energy to the air-fuel mixture more effectively [16].

Subsequently, the temperature increase to tens of thousands of Kelvin causes any vapor present to be raised above its auto-ignition temperature where the fuel has sufficient internal energy to break its carbon-hydrogen bond structures and be oxidized into carbon dioxide, water vapor, and other combustion products [12]. The compression of the mixture, up to the spark event, assists in vaporizing the fuel. The mass of the fuel in the spark plug gap, having started to break down in an exothermic reaction, raises the pressure and temperature of the local molecules [10]. If the reactions are straightforward if the AFR is stoichiometric, however that is hardly ever the case. The actual reaction process is a series of steps that breakdown the fuel in stages to methane and aldehydes. Once the ignition has initiated, the initial flame front near the spark plug is established and heats the unburned layers of fuel-air mixture surrounding the flame front. This is mainly done by radiation but also by convection heat transfer and by mixture motion advancing itself into the flame front [10]. This causes further layers of the mixture to

reach the auto-ignition temperature and thus the flame front advances through the cylinder until in arrives at the physical boundaries [10].

1.3.2. Technologies of Ignition Systems

The most common method used by ignition systems to develop a spark employ a battery system where energy is stored in a capacitor and sent as a high-voltage pulse to the spark plug by means of a special transformer, usually an ignition coil [12]. A capacitive discharge ignition system fully discharges the storage capacitor for each spark event and is described by a peak in voltage and current during the breakdown phase and declining during the arc and glow phases. The breakdown voltage and spark current delivery capability of a CD system is controlled primarily by the design of the associated ignition coil [17]. Sending additional current from a traditional CD coil can only be achieved by reducing the amount of secondary wire or by using a larger gauge of secondary wire. However, by doing this it limits the maximum voltage output due to the increase in distance between the coil winding and the coil core [17]. A coils voltage is a function of the voltage delivered from the ignition module and the ratio of primary and secondary turns in the coil. So, delivering more energy to the ignition coil does not increase the output voltage of the coil.

In order to deliver more energy to the spark plug changes are required to overcome the limitations of the tried and true CD ignition system. The most modern ignition system that has been developed today applies modulated, reinforcing pulses of the primary current and voltage to an ignition coil. Where, instead of completely discharging the system capacitor, a directed energy ignition system uses a constant

voltage source and a high-speed switch to modulate the flow of current through the primary winding of the ignition coil. By doing so, much greater control can be achieved over the spark waveforms, or profiles. Controlling the primary current waveform allows for various spark profiles to be constructed with voltage from the secondary coil reaching over 50,000 volts, while simultaneously delivering the ability to shape the secondary current waveform. The total energy that can be delivered by this system is in excess of 20 times that present in the CD ignition system [17]. It is this directed energy ignition system that will be investigated to determine what, if any, improvements can be measured in the performance of a single-cylinder natural gas engine.

Previous testing done with this directed energy ignition system on a Cooper-Bessemer GMV-4T in a lab environment for two load conditions. Results at full load showed that the combustion heat release was noticeably more rapid than that of the traditional CD ignition system. Lean misfire limit was also extended significantly by reaching stable operation at leaner air-fuel ratios. By extending the lean misfire limit, NOx emissions were able to be significantly reduced from 1.84 g/bhp-hr at an equivalence ratio of 0.655 to 0.95 g/bhp-hr at an equivalence ratio of 0.621, a 50% reduction overall [18]. Furthermore, brake thermal efficiency was also increased by nearly 1% and a reduction 3.5% in fuel consumption. The stability of the engine was also able to be improved at all operating AFRs, including the ultra-lean mixture ratios approaching 0.620. In terms of the relative stability values, the COV of IMEP was able to be reduced by nearly 50% with the directed energy ignition system at all operating air-fuel ratios [18].

The partial load case for the GMV-4T revealed superior performance over the CD ignition spark across the air-fuel ratio range. The BTE of the engine was approximately 1% higher with the directed energy system and the NOx was able to be reduced within the range of 35-50%. Combustion stability mirrored that of the full-load tests in its ability to improve the stability over a given range of air-fuel ratios that were not possible with the CD ignition [18]. These results yielded promise for the directed energy ignition system during its development period, hence warranting further study on engines such as the large-bore single cylinder at AERL.

1.3.3. Ignition Optimization

For every engine an ignition system must be configured correctly to ensure combustion occurs at the most effective time every cycle. This is accomplished by making sure the timing, spark plug geometry, and energy discharge are designed to extract the most work out of every power stroke. With the use of high energy ignition systems, the correct application of the technology must be used to ensure reliability. In situations where the spark profile is not matched with the flow fields between the electrodes and the thermodynamics of the combustion chamber, damage to the electrode surfaces of the spark plug and inadequate extension of the flammability limit are a highly probable result [17].

The combination of the flow velocity acting on the spark arc and the spark waveform are the primary culprits for local heating of the electrode surfaces. When a specific volume of the electrode reaches temperatures that are above the melting point but below the sublimation point is when a pool of molten material is formed [12, 18]. At

the end of a spark event, the surface tensions and electrostatic forces present in the spark plug gap can cause the molten material to solidify into a bead and grow into a whisker [15]. With the proper application of CFD an appropriate spark profile can be matched to the velocity flow fields present in the vicinity of the spark plug gap. This optimization can help to maximize ignitability of a mixture while also preventing damage to the electrode surfaces, thus reducing the potential for misfire. Optimized profiles can maximize ignitability and extend the lean misfire limit to achieve desired performance attributes including lower engine emissions while maintaining durability and reliability of the engine [15].

It should be emphasized that there are no trends that can be applied to all engines for ignition energy relating to performance. There have been conflicting results from many researchers on as to how to improve combustion by spark energy. There is an agreement though that the spark plug gap is a stronger determinant of engine performance than spark energy [19]. The results presented by members of the research community can be accepted though, as the culmination of the results helps to explain short- and long-duration spark events. The shorter duration spark has a better thermal conversion efficiency, and can overcome in-cylinder variations by reliable ignition and accelerated flame kernel development. In contrast, the long-duration discharge is successful as it provides a time frame long enough to mask the effects of in-cylinder variations. A large spark plug gap is similarly beneficial since it increases the likelihood of a favorable combination of turbulence and mixing of the air-fuel mixture within the gap [13].

1.4. Objective

Humanity continues to become more self-conscious about energy is utilized and the possible effects they can have on the environment. It is this motivation that drives the need to improve the performance of the legacy natural gas engines that have been in operation for many decades. With the demand and production of natural gas continuing to rise, it is more important than ever to develop and refine new means of cleaner engine technology. The entire natural gas industry must comply with the increasingly stringent emissions regulations, and natural gas compressors are certainly a part of the necessary improvements. This study aims to improve the range of stable operation and improve emissions at the most fuel-lean operating condition for the Ajax E-565 using a directed energy spark ignition system. The approach will be to conduct spark timing sweeps at a single speed and load, at multiple configurations of spark duration and current, for a standard spark plug and one with an embedded capacitor.

2. EXPERIMENTAL METHODS

2.1. Procedure for Spark Timing Sweep

2.1.1. Methodology for Traditional Spark Plug

The variables that will be in consideration for this investigation include: engine speed, engine load, spark timing, spark duration, and spark current. All test cases will be conducted at an engine speed of 500 RPM and an engine load set to 50% of the maximum load allowable on the engine. These two parameters set the engine in its most fuel-lean operating condition. The spark plug being tested is a Champion W18, with a 22 mm diameter and an electrode gap of 0.025 in. This is the spark plug that is typically used for the AJAX.

The spark timing is set digitally using the interface provided with the directed energy ignition system. Timing values selected include: 6.5, 11.5, 16.5, and 21.5 CAD BTDC. The recommended spark timing for the engine is 11.5 CAD BTDC, thus allowing for the advance of timing by 5 and 10 CAD and retarding by 5 CAD [20]. It was initially planned to retard from nominal timing by 10 CAD as well, however the engine may have been damaged due to extreme pre-ignition. A specific spark duration and current are also set using the digital interface. This digital interface, shown in Figure 6, communicates signals between a computer and the ignition system via a RS-485 module and serial port cable.

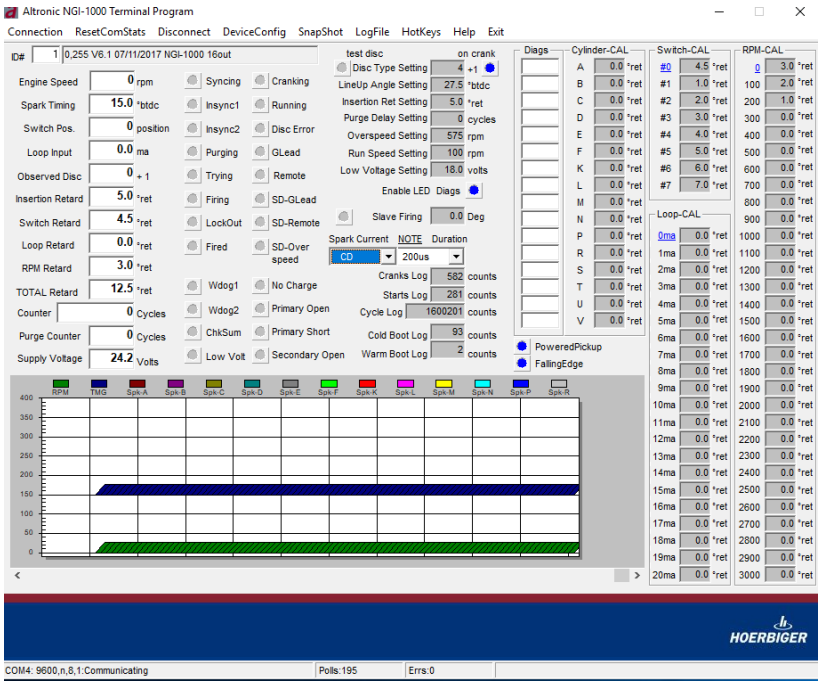

Figure 6: Spark controller UI

The values selected for spark duration include: 200, 600, and 1000 µs. These durations are selected to give a short, medium, and long duration with respect to the capability of the ignition system. All of the spark current values of the ignition system are tested including: 50, 100, 150, and 200 mA. The combinations of spark current and duration settings result in 8 spark profiles that are tested at the 4 spark timings. This results in a total of 32 operating conditions for the traditional spark plug. Each testing condition was repeated a second time, randomly, to ensure repeatability of the results. A sample test matrix for the traditional spark plug are shown in Table 1. Note that the order for the spark timing sweep is always the same, while the duration and current are the values that are randomized. This is done to ensure that each test is collected correctly with the correct file name designation for post-processing of the data. For all test cases,

the engine was given between 5 to 7 minutes to stabilize after an initial 20-30 minute warm-up procedure for the engine.

Table 1: Sample test points for Champion spark plug

Test Number	Engine Speed (RPM)	Engine Load (% of Full Load)	Spark Timing (CAD BTDC)	Spark Duration (µs)	Spark Current (mA)
1	500	50	1.5	200	50
2	500	50	6.5	200	50
3	500	50	11.5	200	50
4	500	50	16.5	200	50
5	500	50	21.5	200	50
6	500	50	1.5	600	50
⋮	⋮	⋮	⋮	⋮	⋮

One parameter that is not to be held constant for this study is the spark energy for each change in spark profile, whether the change be spark current or duration. The limitations of ignition system only allow for specific values to be selected from a drop-down box on the ignition controller UI. If energy were held constant at each change in the spark profile, to determine whether duration or current might have a larger impact on engine performance, the profiles that meet the requirements to do so would only cover 25 percent of the energy discharge capability of the ignition system.

Instead, a different approach to the study is taken by utilizing the full range of the ignition system's discharge capability through spark plug, while disregarding changes to

spark energy. Selecting the three durations and the four spark currents allow for 95 percent of the energy discharge capabilities to be tested. Using combinations of these test points will allow for a broader view of the performance trends that would not be possible with holding the energy constant for each profile change.

2.1.2. Methodology for Capacitor-Embedded Spark Plug

The test procedure is nearly identical for the second spark plug being tested as it was for the Champion W18. This plug is an Enerpulse is a 12 mm NGG1 NR with an electrode gap of 0.055 in. Because this plug is significantly smaller in diameter than what would normally screw into the head of the AJAX, an adapter was used to seat it. This spark plug also bears another component not found in the Champion plug, that being a capacitor. A comparison of the Champion W18 and the Enerpulse NGG1 NR with its adapter can be seen in Figure 7.

Figure 7: Champion W18 and Enerpulse NGG1 NR with adapter

The one difference in the test matrix, when compared to the traditional spark plug, is that only the ignition timings of 6.5, 11.5, and 16.5 CAD BTDC are collected.

Furthermore, the spark timing sweeps are done for the same spark current and duration profiles. Cases of advancing or retarding by 10 CAD are not included as the Enerpulse spark plug is simply being assessed to see if the capacitor embedded in the plug produces any variation in the performance of the engine. The total number of operating conditions for the Enerpulse plug is 24, with each test once again being collected a second time to ensure repeatability.

2.2. Data Collection and Analysis for Both Spark Plugs

In order to quantify the performance of the directed energy ignition system and any impact it may have compared to CD ignition; various parameters will be assessed in the analysis. The primary goals being improved stability and reduced emissions.

Assessing stability can best be determined by observing the cylinder pressure data, to see how combustion is reacting to any changes at the spark plug. The pressure data can be used to determine COV of IMEP, rate of heat release, peak pressure locations, and determining the beginning and end of every combustion event. The cylinder pressure data is what might best be known as the backbone for all data collected from the engine.

The other aspect of assessing the ignition system is any difference in emissions performance. By quantifying the combustion products of CO, CO_2, NOx, THC, and O_2 at each test condition a conclusion is able to be drawn about whether or not the engine burns cleaner by having greater control over the spark.

2.3. Equipment

2.3.1. Engine

The engine used to conduct the test for this research is an Ajax E-565. This engine is a two-stroke, single cylinder, naturally aspirated engine. It has an 8.5” bore and a 10” stroke, thus giving a displacement of 9.3 L [20]. Figure 8 shows the engine with the directed energy ignition system installed.

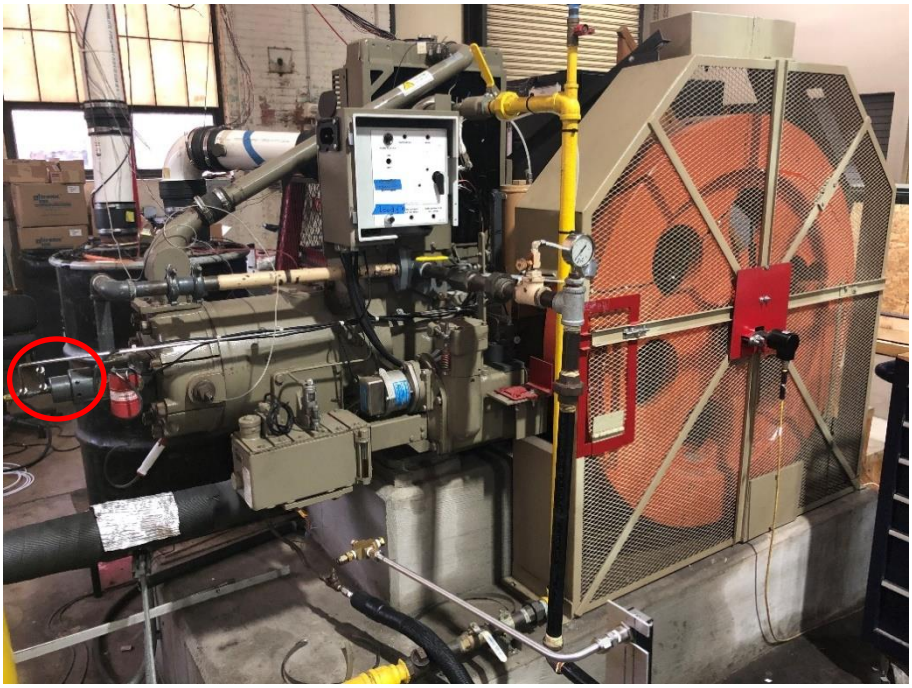

Figure 8: Ajax E-565 setup at Texas A&M University

It should be noted that this engine is also equipped with a direct injection system, that can be seen in the red circle to the left of and behind the red ignition coil. The engine is typically fueled through the stuffing box via the yellow natural gas line shown in Figure 8. The composition of the fuel can be found in Appendix B. A detailed description of the current Ajax engine configuration can be seen below in Table 2.

Table 2: Detailed description for Ajax E-565 [20]

Bore x Stroke	8.5” x 10”
Torque	400 ft-lb
Rated Speed	525 RPM
Recommended Speed Range	300-525 RPM
Compression Pressure	145 PSI
Compression Ratio	6:1
Ignition System	Altronic NGI-1000
Fuel Injection	Direct Injection
Weight	4420 lbs.

2.3.2. Ignition System

The ignition system that will be assessed in this study is an Altronic NGI-1000. It replaces the Altronic I ignition system that originally was installed on the Ajax E-565. Figure 9 shows the NGI-1000 mounted within the engine control box.

Figure 9: NGI-1000 ignition system mounted to Ajax E-565

This ignition system is installed on the engine with a timing disk, mounted to the crankshaft, and a magnetic pickup sensor used to relay the timing signal to the NGI-1000 [21]. A standard ignition coil is also used between an output harness and the spark plug with a resistor lead connecting the coil to the spark plug terminal.

2.3.3. Dynamometer

The dynamometer used in conjunction with the Ajax E-565 is an eddy-current Taylor DEA 150. Its limits include a 150 HP, 3500 RPM full load capacity; meaning that it far exceeds the capabilities of the engine during operation [22]. The load is controlled by a potentiometer mounted to the engine control panel and the readout is displayed on a Fluke multimeter in volts. Physical specifications for the dyno can be found below in Table 3 and the orientation, in conjunction with the Ajax, can be seen in Figure 10.

Table 3: Specifications for Taylor DAE150 [22]

Heat Load Emitted by Dyno Per Hour	382,000 BTU	115 kW
Height (not including cement base)	49 in	124.5 cm
Width of Mounted Holes	39.13 in	99.39 cm
Length	17.5 in	44.45 cm
Weight	1300 lbs.	590 kg

Figure 10: Taylor DAE150 connected to Ajax E-565

2.3.4. Data Acquisition System

The DAQ is used to record all data besides that of the emissions, which will be discussed in the next section. The system is comprised of individual National Instrument components that are mounted to a NI cDAQ. The modules collect data from signals of: pressure transducers (in-cylinder, intake, and exhaust), intake and exhaust thermocouples, and fuel flow rate. All of this data is collected and recorded at every quarter degree for the entire 360 degrees to complete a single cycle, resulting in 1440 data points per revolution. Each test point collects data for 300 consecutive cycles. The signals are compiled by a code developed in MATLAB by members of AERL.

2.3.5. Emissions Bench

The exhaust products of the Ajax E-565 are analyzed by a Horiba MEXA-7100D emissions bench. This bench has the capabilities to measure the following constituents: CO, CO_2, THC, NOx, and O_2. Specifications of the individual analyzer can be found in Appendix C.

Measurement of CO and CO_2 is done via NDIR detectors. Each constituent gas in a particular sample will absorb some amount of infrared at a particular frequency. By sending infrared light through a sample (containing either CO or CO_2), and measuring the amount absorbed by the sample at the necessary wavelength, a NDIR detector is able to measure the volumetric concentration of CO or CO_2 in the sample. A chopper wheel is mounted in front of the detector continually correcting the offset and gain of the analyzer and allows for a single sample to measure the concentrations of both species [23].

NOx, specifically NO, is measure by a CLD. The reaction between NO and O_3 (ozone) emits light. This reaction is the basis for the CLD in which the photons produced are detected by a photo multiplier tube. The CLD output voltage is proportional to the NO concentration [24].

THC is measured using the industry standard analyzer known as an FID. This analyzer works by first introducing the sample gas into a hydrogen flame. Any hydrocarbons in the sample will produce ions when they are burnt. Ions are then detected using a metal collector. The current across this collector is proportional to the rate of ionization, which in turn reflects on the concentration of hydrocarbons [25].

For the traditional spark plug, the values for each emission gas is recorded by visual inspection of the UI for a minimum and maximum value for a period of 30 seconds. The two values are then averaged together to give a single number per test point. Before beginning collection of the data for the capacitor-embedded spark plug, the MEXA was upgraded to have the capability to record data automatically. This allows for all emissions data to be collected every 0.1 seconds for a 60 second time period [26]. The data is then saved to a USB drive, which can then be transferred to another computer for data analysis. Unfortunately, there was not enough time or resources to repeat test matrix, twice, for the traditional spark plug. A view of the MEXA interface can be seen below in Figure 11.

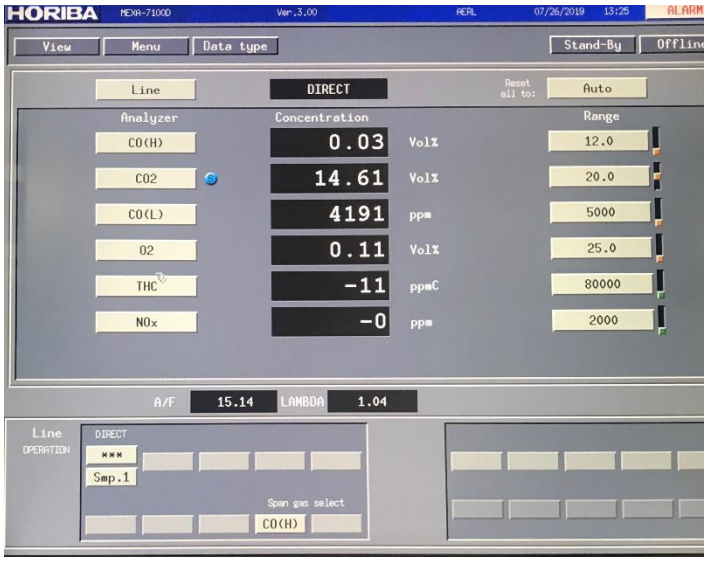

Figure 11: User interface for Horiba MEXA-7100D

3. RESULTS AND DISCUSSION

3.1. Traditional Spark Plug

Data collected from in-cylinder pressure and emissions are done so only upon complete stabilization of the AJAX for a particular operating point. The stability is confirmed by the engine speed oscillating within a range of 2-5 RPM for 90 seconds. All test points were selected randomly during the initial and secondary trials to ensure repeatability and minimized any effects of the previously collected test point.

Selecting the engine to operate at half-load and a speed of 500 RPM is done so to see if the engine can operate at the lean condition with reliable combustion and reduced emissions, especially NOx. In testing at these operating conditions for each spark timing sweep it became immediately apparent what the shortcomings are with a single cylinder, large-bore, slow speed engine. The single cylinder design results in pulsations of the air and fuel, thus creating oscillations in data readings that would not be present in a multi-cylinder engine. Having a large-bore combustion chamber can also be an issue with the air and fuel mixture and the turbulent flows within the cylinder such as the swirl and tumble effects. The homogeneity was found to be a particularly sensitive issue, especially since converting the AJAX to direct fuel injection. This is apparent by the inability to start the engine on the direct injection system below around 65 ºF. The engine will, however, easily start on the premixed fuel injection system that previous studies have used for this engine. Two-stroke engines, especially those that are slow speed, must also deal with the fact that some fresh charge will directly slip through the cylinder and be exhausted without undergoing combustion and thus reducing the

efficiency of the engine. The slow speed itself yields more time for the intake and exhaust ports to be open at the same time and allow this to happen. While the engine is no longer considered to short-circuit fuel directly to the exhaust, the loss of fresh air alone is just as vital to the combustion process.

These factors are a reason why certain parameters, particularly air and fuel flow rates, are either unable to be recorded or have large margins of uncertainty. The air flow rate, at the time that these experiments took place, was believed to be erratic considering the size installed surge tank is for the AJAX and ultimately deemed unreliable for this study. The current surge tank is only 17% of the recommended size for the AJAX, according to Kastner [27]. Fuel flow rate is another measurement that will not give consistent data readings for low load settings for the engine. However, at high loads there are consistent readings. This could be that the surge tank for the direct injection system is too small, but more investigation is necessary to determine why these effects are being seen.

One last point to mention is that use of CFD is quite helpful in optimizing the spark profile. It allows for understanding of the local AFR and flow velocities around the spark plug gap. Unfortunately, a CFD model of the AJAX in its current configuration is not readily available to use for this study. As such the comprehensive test matrix described in the procedure is determined to be the best means of finding the optimum spark profile.

3.1.1. Stability of the AJAX

Analyzing the combustion stability of the AJAX is an essential aspect of determining if an engine is running with consistency in its operation. Variability in cycle-to-cycle combustion has negative effects on emissions, fuel efficiency, and engine performance. The root cause of these issues, specifically for SI engines include local flow velocity near the spark plug gap, turbulence throughout the combustion chamber, fuel quantity, and the residual mass fraction [28]. For the AJAX in particular, some of these issues were previously address concerning it being a single cylinder large-bore engine that operates at slow speeds.

The parameter used to assess the stability is the coefficient of variance of indicated mean effective pressure, or COV of IMEP. IMEP is the net average cylinder pressure that provides the equivalent work of the actual cycle, including all strokes of the cycle. In other words, it is the work produced per cycle divided by the displacement volume per cycle. This normalized parameter allows for different sized engines with varying designs to be compared against each other. The standard deviation of the IMEP divided by the mean of the 300 cycles is the COV is calculated. This value provides a representation of how the work output of the engine varies, with higher percentages indicating lower stability.

In order to see if any trends are in the spark properties, the profiles are arranged by the current sent to the plug. Figure 12, Figure 13, Figure 14, and Figure 15 group the profiles based on the spark currents of 50, 100, 150, and 200 mA, respectively.

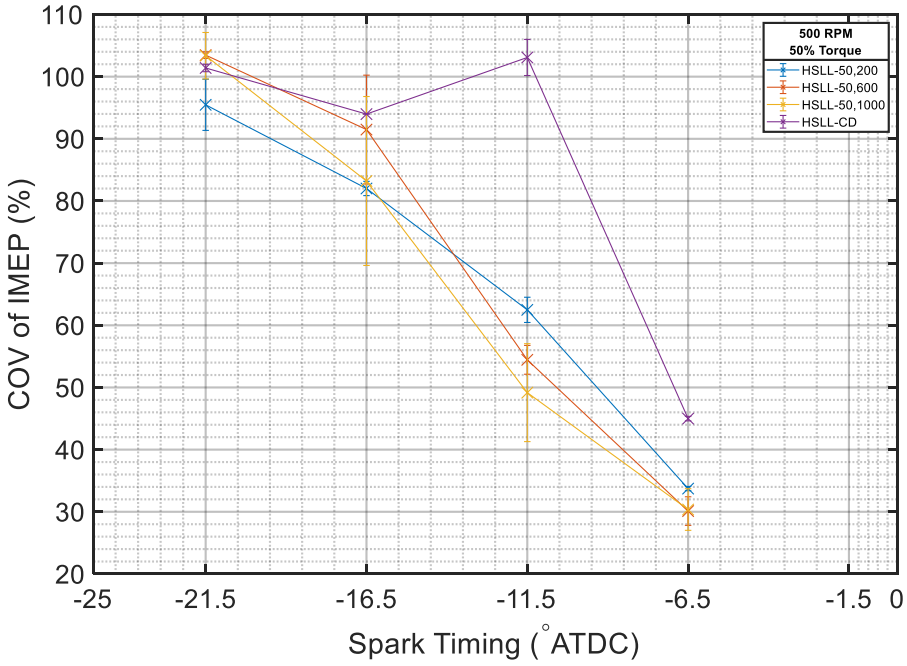

Figure 12: COV of IMEP for 50 mA current and varying duration

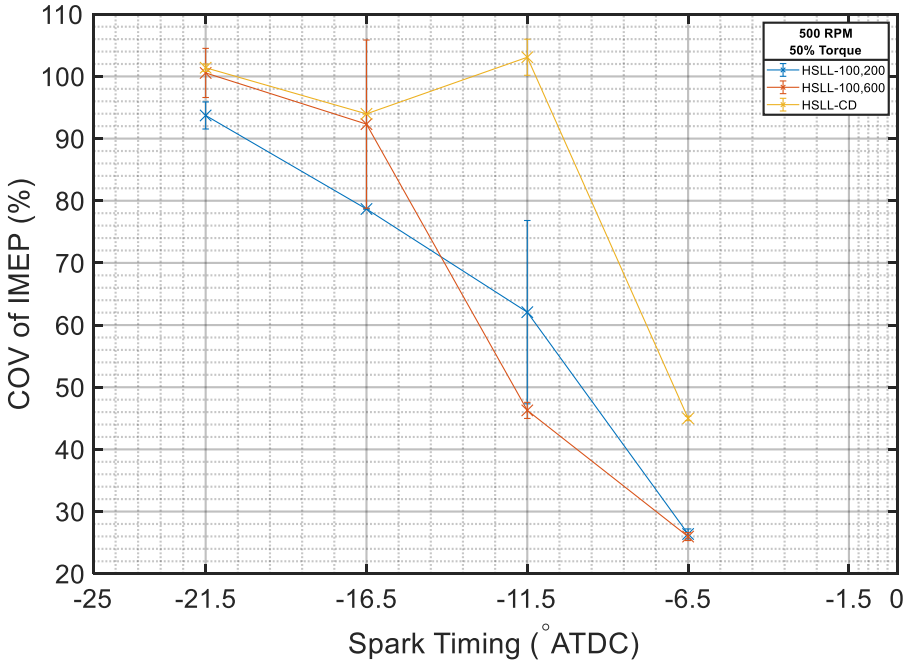

Figure 13: COV of IMEP for 100 mA current and varying duration

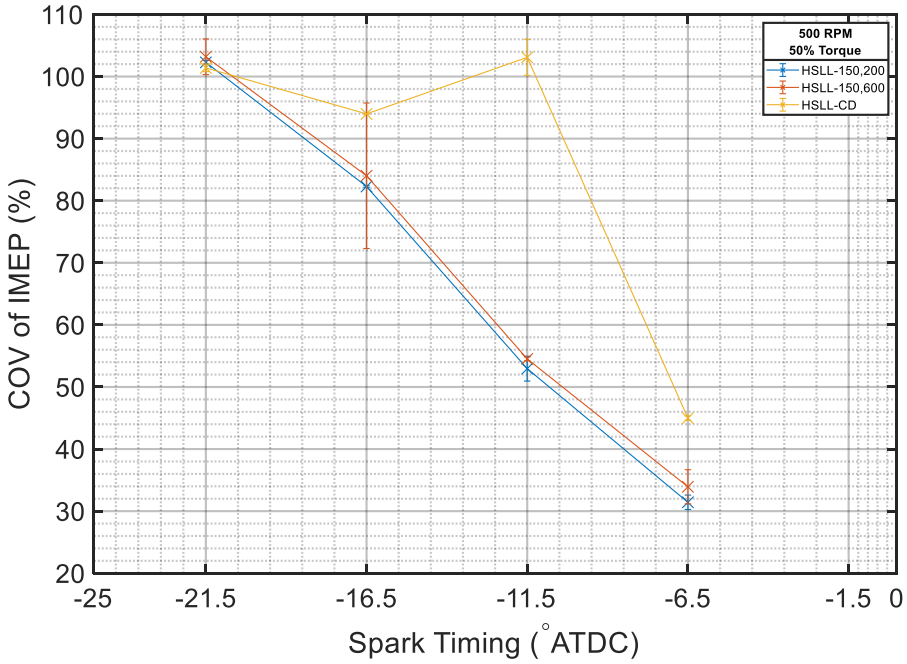

Figure 14: COV of IMEP for 150 mA current and varying duration

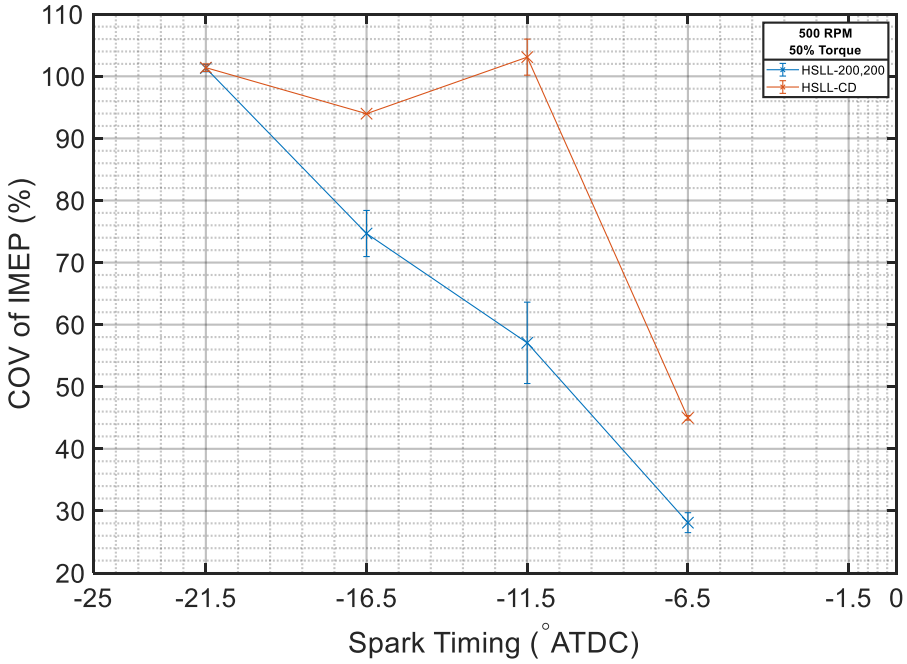

Figure 15: COV of IMEP for 200 mA current and varying duration

Evaluating the entire range of spark profiles, based on constant current, there is no indication of any trend in terms of the stability of the engine. The values of COV of IMEP do follow the trend of increasing stability as the timing continues to retard towards TDC. Each of the error bars represent a 95% confidence interval, or two standard deviations from the mean at each spark timing. This means that when different data set's confidence intervals overlap each other, there is no statistical difference in the spark profiles.

These figures also show that for the cases of -16.5 CAD, -11.5 CAD, and -6.5 CAD ATDC the stability is certainly improved over CD ignition. The profiles with a current of 100 mA, in Figure 13, show improvement for -6.5 CAD ATDC with values of 26% versus the CD value of 44%. Similarly, for -11.5 CAD ATDC, the spark profile of 150 mA with 200 µs duration in Figure 14 results in a COV of IMEP of 53% while the CD ignition produces a value of 103%. At -16.5 CAD ATDC, in Figure 15, with a spark profile with 200 mA and 200 µs produces a value of 75% compared to the 94% when using the CD ignition. The most advanced case did not produce any notable improvement using the directed energy ignition system, within the margin of uncertainty. Furthermore, because it can be shown that there is no particular profile that is superior to all other across the spark timing sweep. This is consistent with what has been discovered by many other researchers investigating the modulation of spark energy [15, 19]. Matching the absence of trends seen with constant current, comparing the timing sweep on a constant duration basis also indicates no trends. As there are no

significant additions with the constant duration figures, they are placed Appendix A for reference.

Due to the inability of optimizing the spark profile for the AJAX with CFD, this comprehensive sweep was used to search for the most ideal profiles at each timing, for this particular speed of 500 RPM and 50% load. In association with the high COV of IMEP values seen for this speed and load, the number of misfires is considerably higher than that when operating at rated speed and a higher load value. While the results are indeed an improvement in combustion stability, the performance of the engine is still not what would be considered acceptable for extended operation. The number of misfires and severe pre-ignition following a misfire, especially for -6.5 CAD, would more than likely cause damage to components of the engine if it were to operate at these parameters in the field. COV of IMEP values need to be below 20% for the AJAX to be at stable operation [29].

Because of the misfires and incomplete combustion, emissions are significantly affected by the lower in-cylinder temperatures and unburned mixture exiting the exhaust, particularly NOx and THC. The emissions results for the traditional spark plug will be discussed in the following section.

3.1.2. Emissions

3.1.2.1. Nitrogen Oxides

NOx emissions are of great importance, especially in the natural gas sector, as they are one of the main constituents under scrutiny by tightening regulations. The results shown below do have high levels of uncertainty, though this is typical nature for

this particular engine as has been shown in past research [29]. Since the AJAX is operating at its most fuel-lean condition of high speed, low load; the values of NOx should be relatively lower than those seen in at common operating conditions of rated speed and high load. The NOx emissions can be seen below in Figure 16, Figure 17, Figure 18, and Figure 19 for constant currents of 50, 100, 150, and 200 mA, respectively.

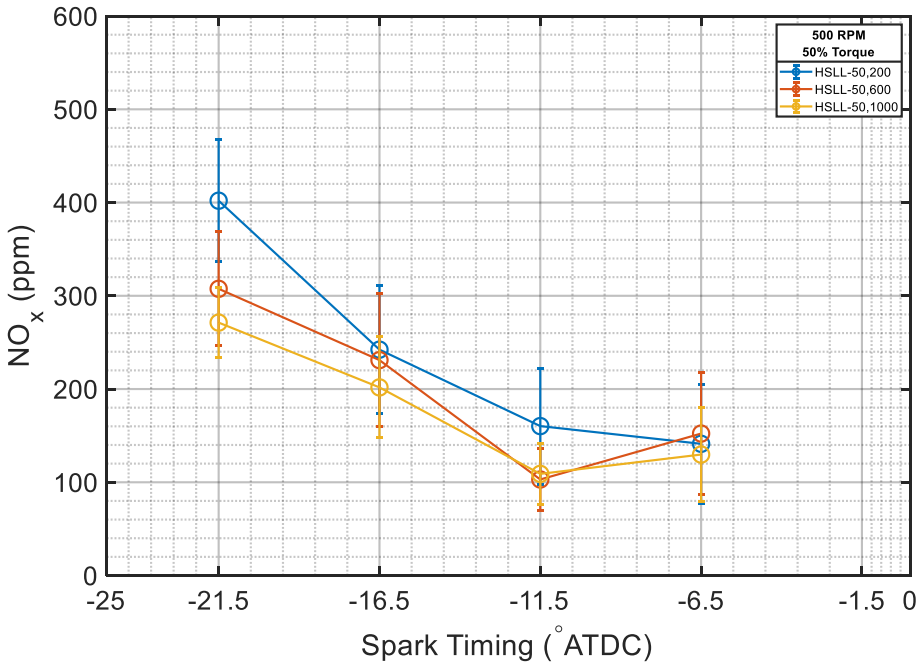

Figure 16: NOx emissions for 50 mA current and varying duration

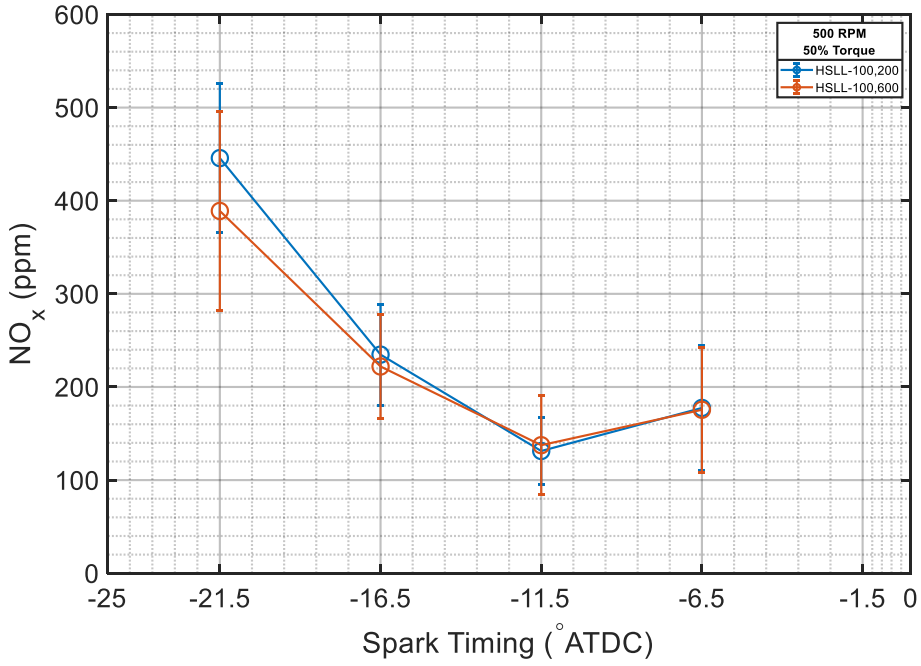

Figure 17: NOx emissions for 100 mA current and varying duration

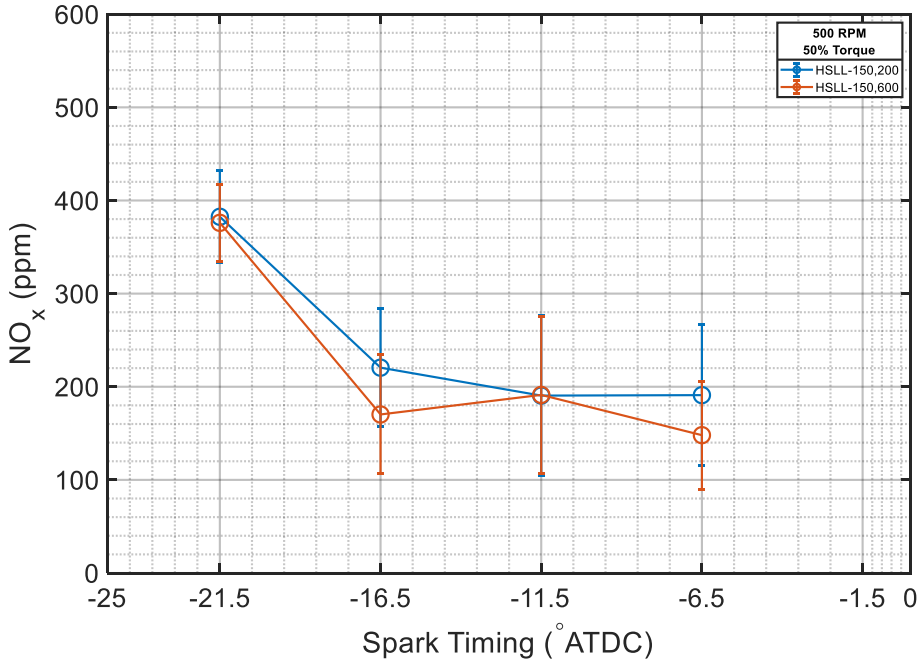

Figure 18: NOx emissions for 150 mA current and varying duration

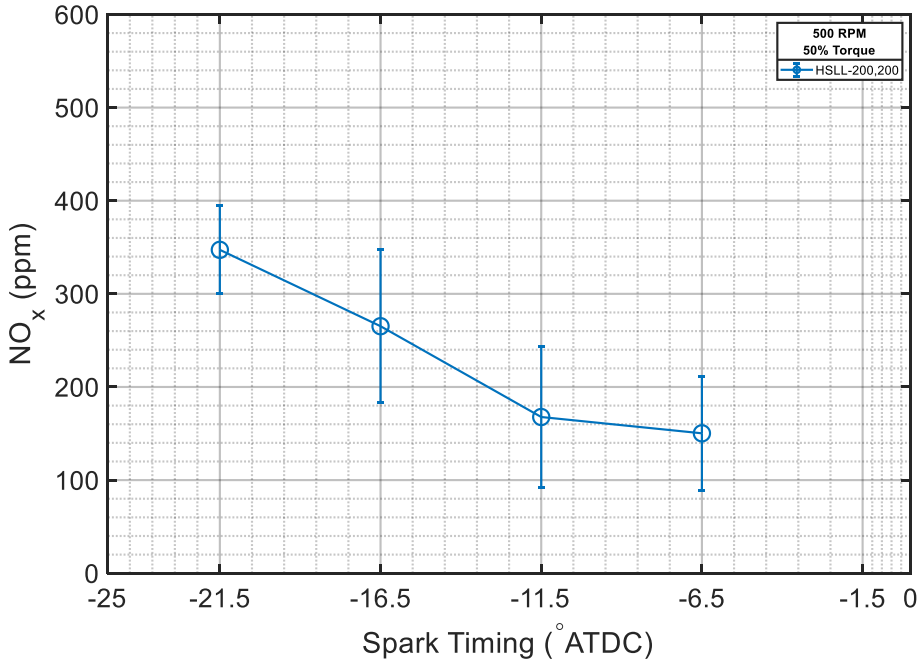

Figure 19: NOx emissions for 200 mA and varying duration

The results of NOx emissions are similar to that of the stability in that there are not trends in varying the spark profiles when holding current constant. The same is true about holding duration constant, with those figures reserved for Appendix A. There is a trend though in decreasing NOx with more retarded spark timing and with that, increasing stability. When the engine becomes more stable, the in-cylinder temperature should be higher due to more complete combustion cycles and thus develop higher NOx emissions. In this instance, the most likely factor for higher NOx emissions is the combination of misfires followed by premature ignition of the mixture. The reasoning for this being that the mixture in the cylinder can go for one or two compression strokes without combustion. The residual gas fraction, in turn, increases along with the temperature. As this fraction gets larger and mixes with the incoming charge, the overall

AFR of the mixture becomes richer [12]. At some point in the compression cycle following a misfire or two, the autoignition temperature is reached somewhere in the cylinder and causes the rich mixture to pre-ignite [30]. This results in substantial increase in pressure and temperature and thus a large production of NOx.

In assessing the data for an optimum profile at each timing, as was done with the COV of IMEP, the uncertainty in the results does not allow for a conclusion to be drawn. Neither changes in current nor duration of the spark profile prove to be of any influence on the NOx emissions of the engine. These high NOx values, disregarding the spark timing changes, can be linked back to the instability of the engine operating at 500 RPM and 50% load. Figure 20 is a live readout of some of the emissions in real-time during a sample test run at these engine operating conditions and provides an explanation for the high levels of uncertainty in the results.

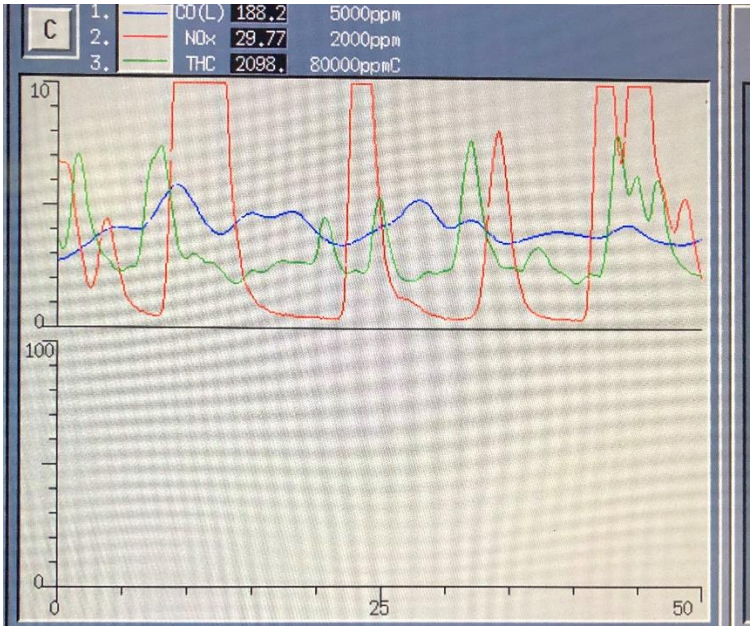

Figure 20: Real-time emissions of AJAX

The red line represents the NOx value, with a generic scale to represent all of the emissions being recorded. The large spikes see for the NOx occur during every pre-ignition event for the engine. When the engine is operating with normal combustion and some misfires, the NOx emissions are much lower, between 0 and 2 on the scale. This trend of seeing spikes is noticed across every spark profile for all spark timings when collecting data. The magnitude of the values in Figure 20, however, do not represent any of the data shown previously in this paper or in the future as this timing was around 5 CAD ATDC (a heavily retarded timing). When operating in the previously stated spark timing range for this study, the spikes in NOx are of lower magnitude.

3.1.2.2. Total Hydrocarbons

Emission of THC for two-strokes in general is mainly attributed to short-circuiting where fuel is transferred immediately from the intake to the exhaust port without undergoing combustion. Much of this issue has been rectified on the AJAX by having a direct-injection system deliver fuel to the cylinder after all ports have been closed. The abolishment of short-circuiting allows for sole analysis of the quality of combustion. The THC measurements for spark profiles holding current constant are grouped below based on their durations in Figure 21, Figure 22, Figure 23, and Figure 24.

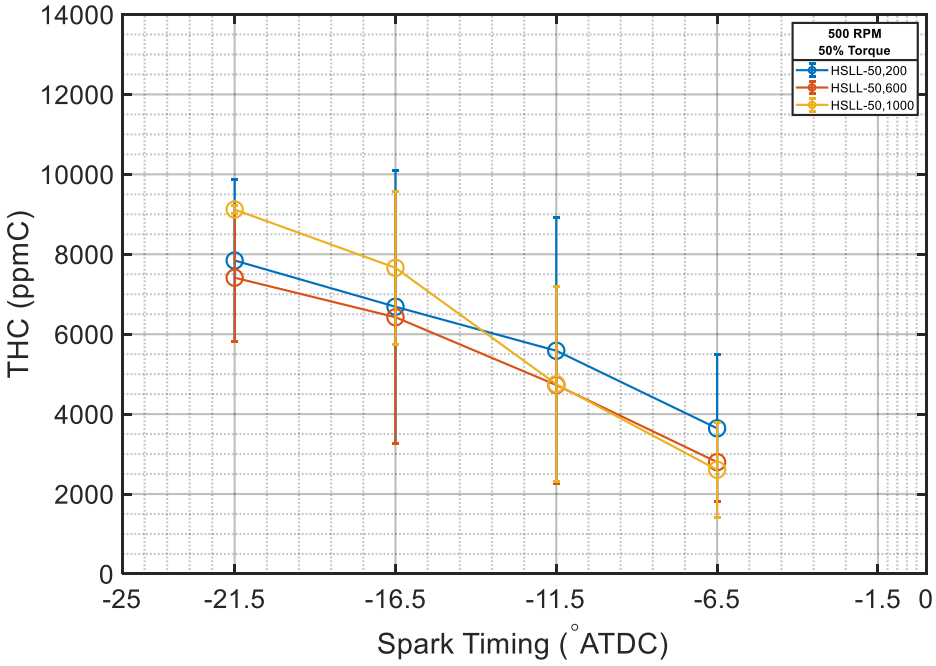

Figure 21: THC emissions for 50 mA and varying duration

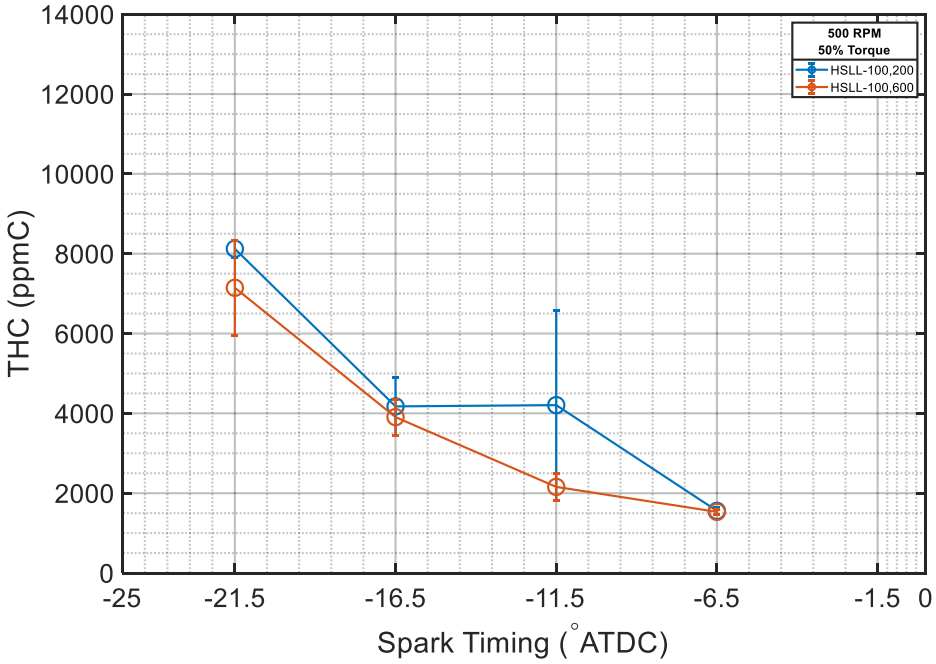

Figure 22: THC emissions for 100 mA and varying duration

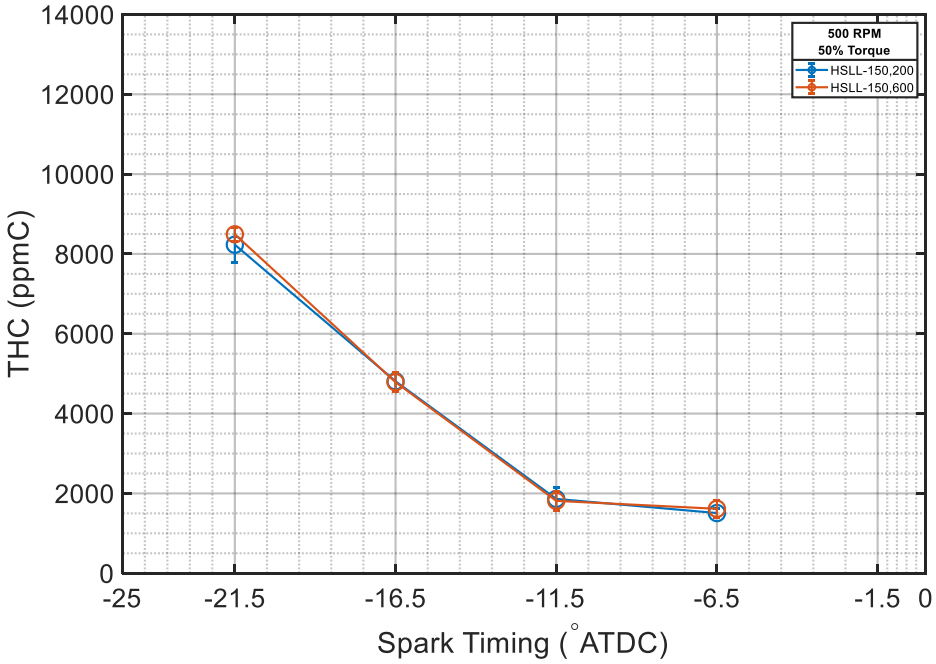

Figure 23: THC emissions for 150 mA and varying duration

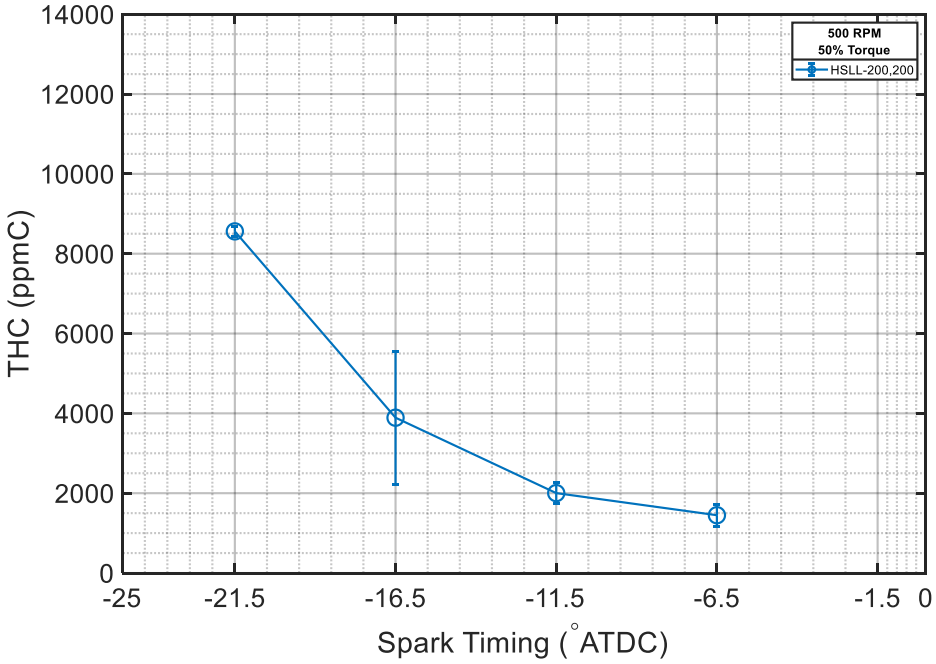

Figure 24: THC emissions for 200 mA and varying duration

Across all spark profiles, the THC emissions decrease as the spark timing moves towards TDC. This trend, fundamentally, can be explained by the stability as it increases with retarded spark timing and, hence, having fewer misfires and pre-ignition events. By combusting more of the air-fuel mixture, less unburned fuel is discharged to the exhaust. It can also be shown that no particular trends are apparent by varying duration and holding current constant. The same can be said for varying current while holding duration constant. The results displayed with constant duration are withheld from the main report, as they provide no further insight, and can be found in Appendix A.

While not particular spark profile proves to be superior over others, certain profiles definitely resulted in higher uncertainty than others. Figure 21 shows the THC for a current of 50 mA with uncertainty ranges of 7000 ppm, which are similar to previous emissions studies on this engine [29, 31]. The other currents do not have such high discrepancies in their THC emissions. The only explanation for the high uncertainty for only the 50 mA spark profiles is the method of obtaining the emissions data. While the means of collected data does present a difficult way of show a fair representative value of the emissions, the method used does provide an extremely conservative representation of the THC output of the AJAX.

Again, just as with the NOx real-time readings seen in Figure 20, the resulting values do not entirely explain the operation of the engine entirely. When the engine misfires, there is a sharp spike in the THC reading, this is then followed by pre-ignition of combustion during the next compression stroke, thus giving the high reading in NOx. The combination of the unreasonably high stability and instances of extremely high

emissions of NOx and THC show that the AJAX is very much outside of the acceptable range at which it should operate in the field.

3.1.2.3. Carbon Monoxide

Carbon monoxide is a colorless and odorless gas that can silently kill by inhibiting the binding of oxygen to red blood cells, which instead bind to the CO [32]. During the combustion process, CO production is attributed to an AFR that is too rich with fuel, resulting in incomplete combustion. Figure 25, Figure 26, Figure 27, and Figure 28 show the CO emissions for the spark profiles with constant currents of 50, 100, 150, and 200 mA, respectively.

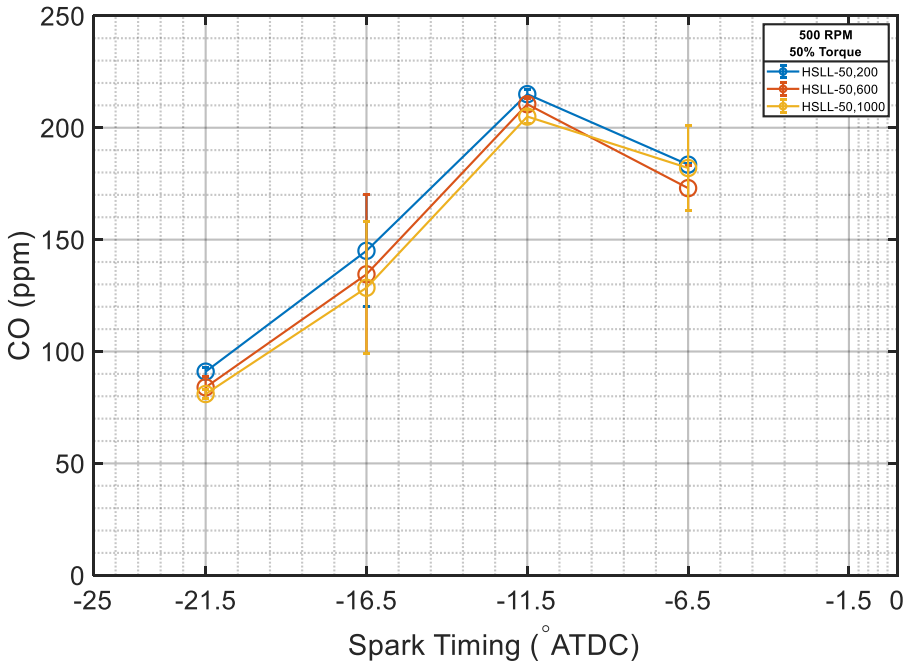

Figure 25: CO emission for 50 mA and varying duration

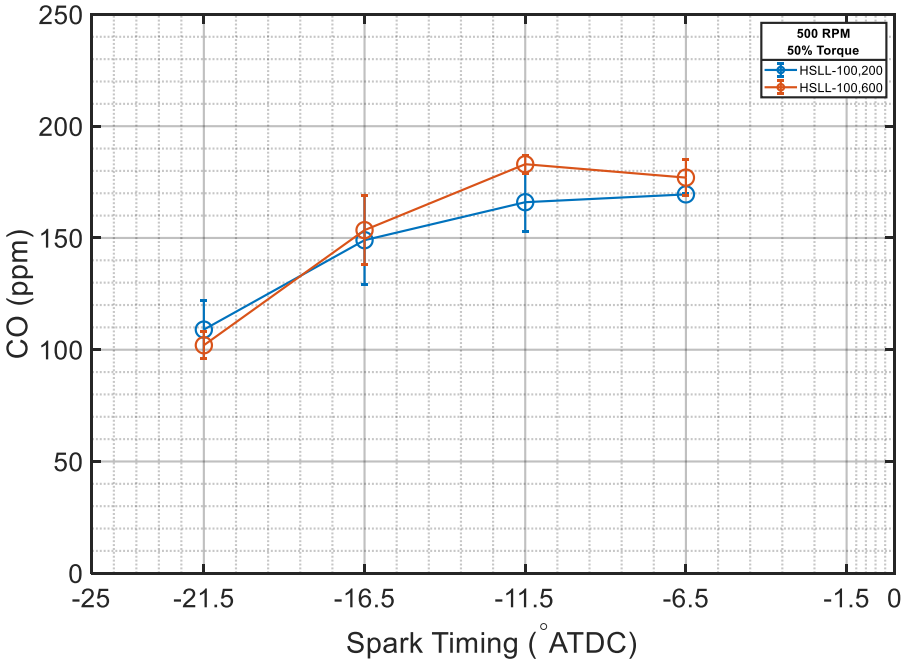

Figure 26: CO emissions for 100 mA and varying duration

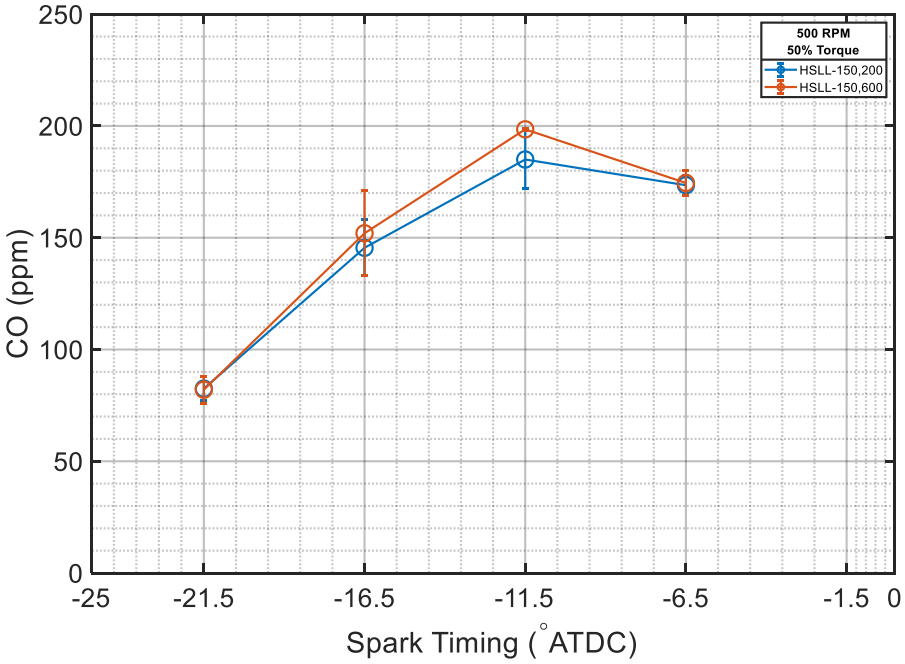

Figure 27: CO emissions for 150 mA and varying duration

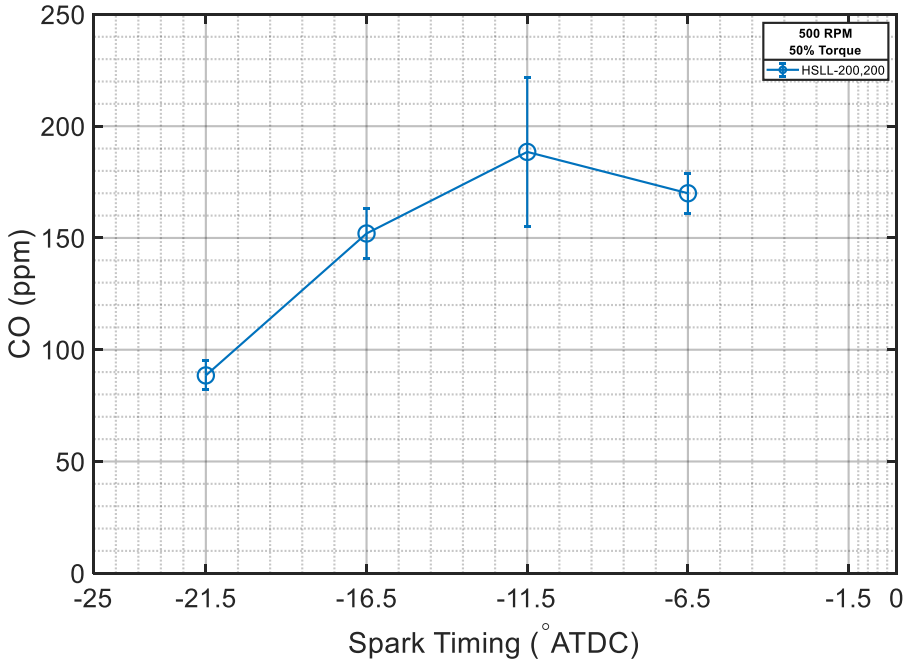

Figure 28: CO emissions for 200 mA and varying duration

The results display a consistent movement of increasing to the nominal timing of -11.5 CAD ATDC and then slightly decreasing afterwards. In theory, this result is reasonable since increasing the amount of retard to the spark timing results in an increase in the amount of fuel being delivered to the engine. Another explanation, that can only be seen when varying the load, is that the combustion energy at low loads is insufficient to complete the reaction to CO_2 and thus "freezing" the products as CO [29].

In assessing the spark profiles for optimum configurations, the uncertainty restricts a concrete conclusion from being deduced. Once again, no trends can be concluded from these results, as is also the case with holding the duration constant and varying the current. The figures for constant duration are held for Appendix A.

3.1.2.4. Carbon Dioxide

Considering the products of an ideal stoichiometric combustion between a hydrocarbon and oxidizer, CO_2 and H_2O are the only constituents [10]. The AJAX always operates with lean AFRs as it is a lean-burn engine. This suggests that as the spark timing is swept from most advanced to most retarded, and thus increasing the amount of fuel admitted, the combustion process should be more complete and therefore should have higher amounts of CO_2. The results of the CO_2 emissions can be seen in Figure 29, Figure 30, Figure 31, and Figure 32, again separated by the current for each spark profile.

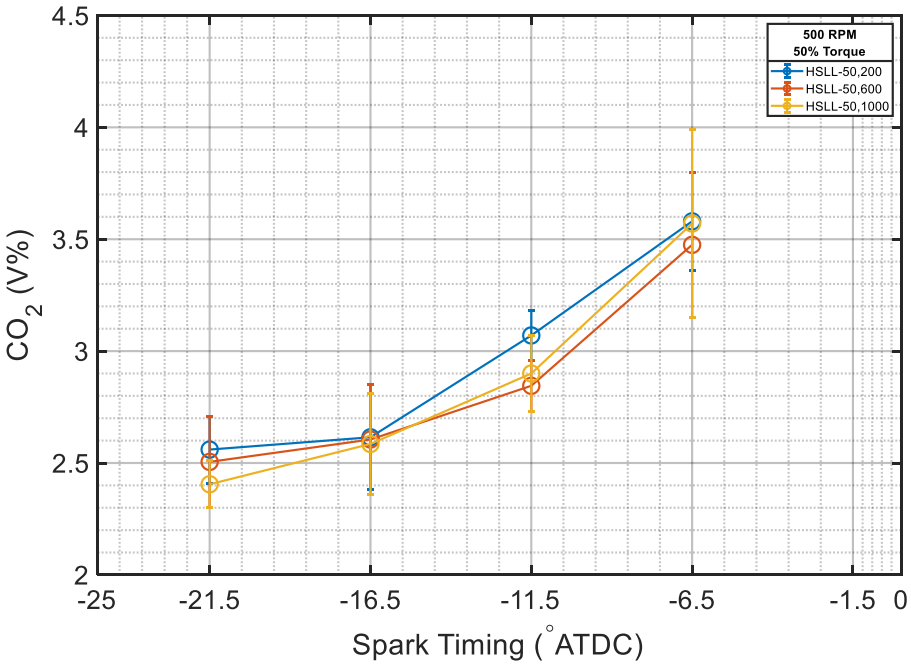

Figure 29: CO_2 emissions for 50 mA and varying duration

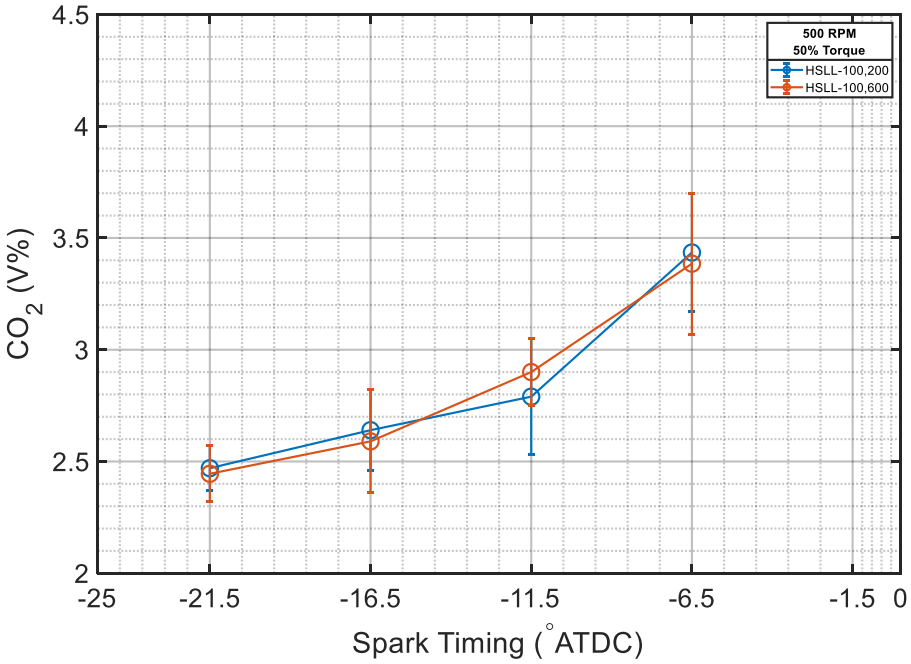

Figure 30: CO_2 emissions for 100 mA and varying duration

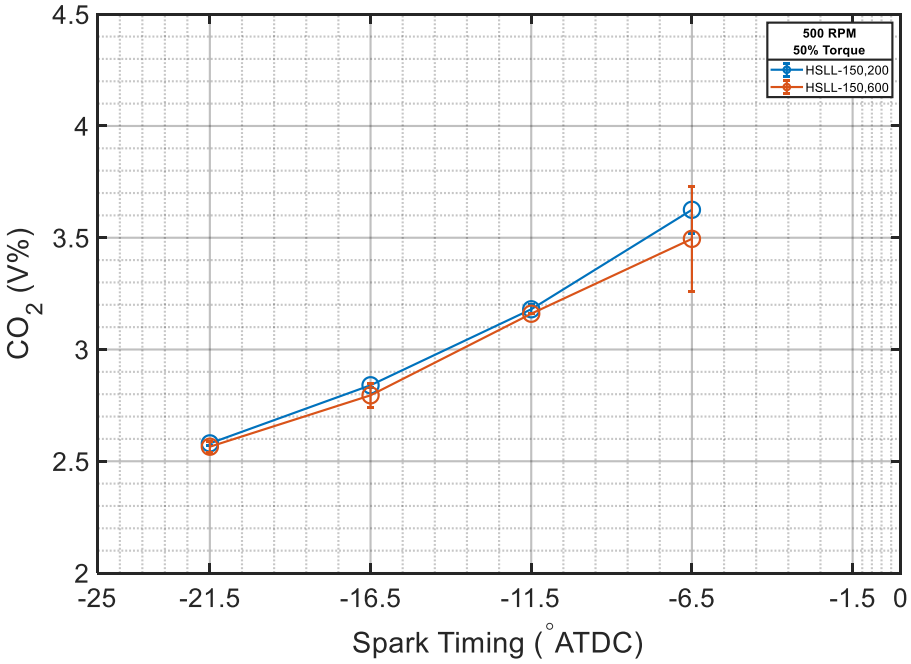

Figure 31: CO_2 emissions for 150 mA and varying duration

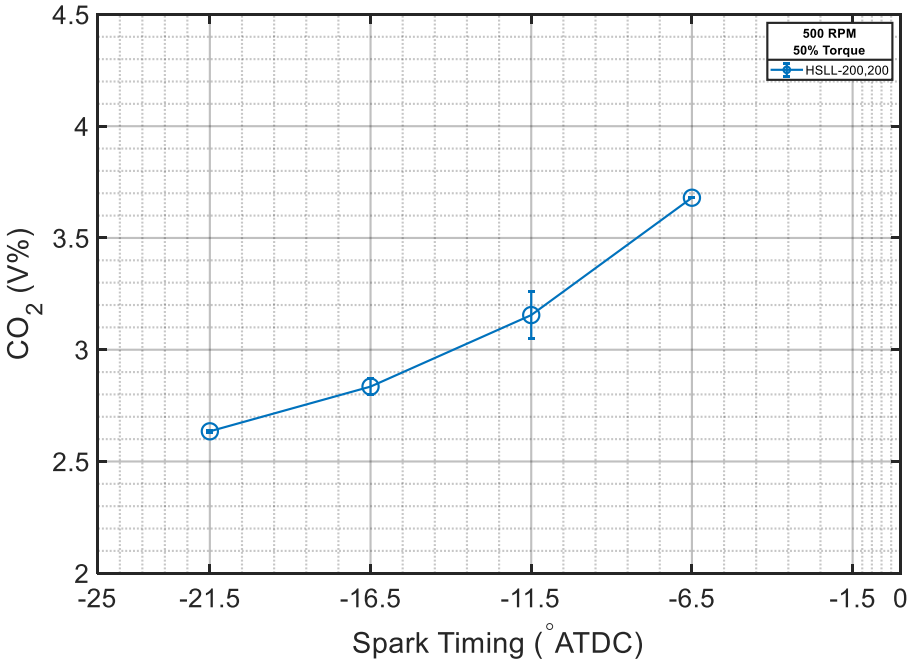

Figure 32: CO_2 emissions for 200 mA and varying duration

The results do follow the expected trend of increasing CO_2 concentration with increasing amount of spark retard. Each spark profile is within each other's range of uncertainty, suggesting no trends between various spark profiles for varying spark duration. The same can be concluded for constant current; the data presented by a profile's duration can be found in Appendix A.

The same relative uncertainty ranges seen in the THC results are shown with CO_2 emissions. Profiles with 50 mA currents, in Figure 29, have much more uncertainty that those for the other spark configurations. However, when comparing the other profiles with smaller uncertainty, they still overlap each other. The two noticeable results are the 150 mA and both 200 and 600 µs durations. The profiles have a relatively small uncertainty and the most optimum average results for the timing sweep.

3.1.2.5. Oxygen

The final measurable exhaust emission is O_2, a fair indicator of the AFR of the engine. With no reliable means of determining AFR before the charge is admitted to the cylinder, this is the best technique to back-calculate a value and confirm the validity of the other emissions results. Figure 33, Figure 34, Figure 35, and Figure 36 present the O_2 emissions based on constant current discharge through the spark plug.

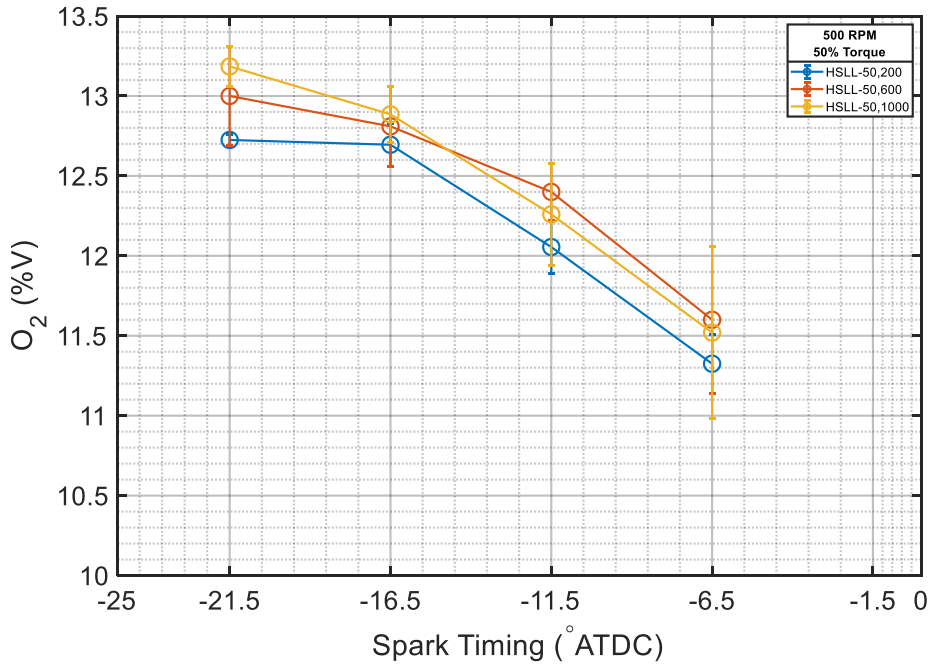

Figure 33: O_2 emissions for 50 mA and varying duration

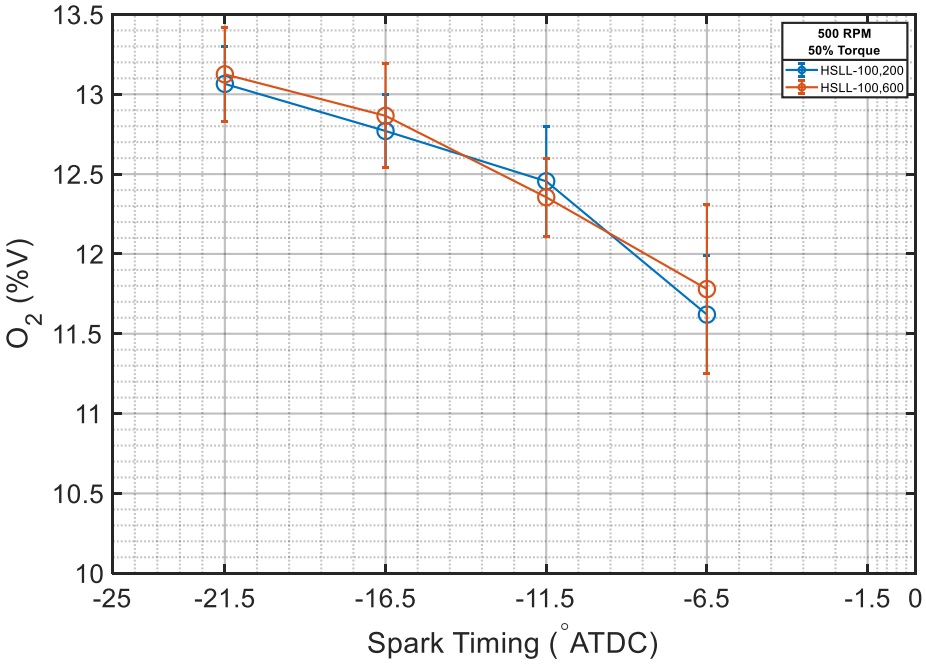

Figure 34: O_2 emissions for 100 mA and varying duration

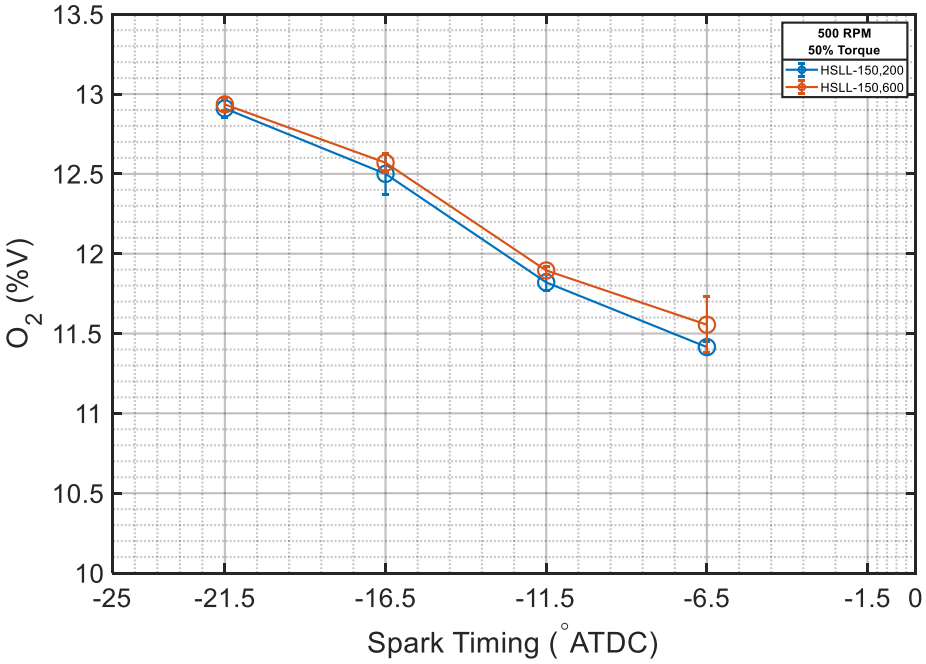

Figure 35: O_2 emissions for 150 mA and varying duration

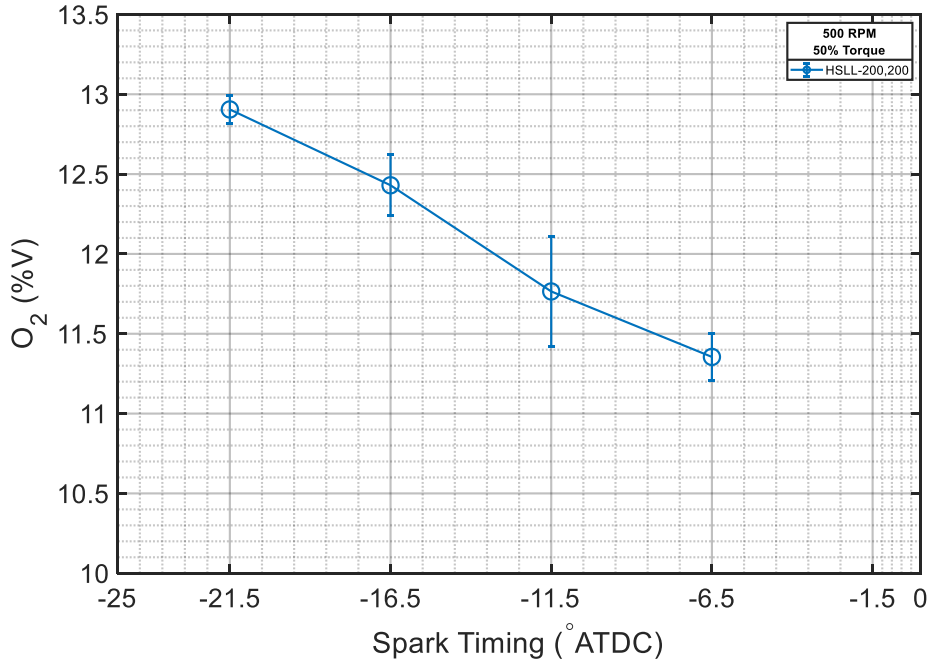

Figure 36: O_2 emissions for 200 mA and varying duration

Across all spark profiles the O_2 percentage emitted is as would be expected, considering the results of the other exhaust constituents. As the spark timing transitions from -21.5 CAD to -6.5 CAD ATDC, the O_2 amount reduced in the exhaust. This trend is inversely proportional to the results of CO_2, meaning an increase in AFR. COV of IMEP also reinforces that as the engine gets more stable, when the spark timing shifts closer to TDC, the stability increases as a result of being closer to stoichiometric conditions in the cylinder.

In assessing the effect of the various spark profiles, no trends are able to be deduced either for constant current or constant duration. The spark profile of 150 mA current with either a duration of 200 or 600 µs proves have to relatively repeatable results. This reinforces the small uncertainty in the same profiles' CO_2 emission results

in Figure 31. As a whole though, the uncertainty is too high and the emissions have such similar values support the conclusion that spark profile changes have very little impact on emissions for the high speed, low load operating condition for the Ajax.

3.2. Capacitor-Embedded Spark Plug

In addition to testing the Champion W18, a capacitor-embedded spark plug is of interest as it has never been coupled with a directed energy ignition system before now. As discussed in the methodology for the capacitor-embedded spark plug, this is designed for engines of smaller size. No Enerpulse plug is large enough to fit in the AJAX without an adapter. As such, the center electrode is 0.5 mm smaller in diameter than the Champion W18, along with a shorter reach into the cylinder by 2.2 mm.

3.2.1. Stability of the AJAX

The first assessment metric is the stability of the engine, quantified by COV of IMEP. To establish a baseline, the capacitor-embedded spark plug was used in the CD setting on the ignition system software, instead of comparing to the baseline from the traditional plug. Figure 37, Figure 38, Figure 39, and Figure 40 show the stability for currents of 50, 100, 150, and 200 mA with varying duration, respectively.

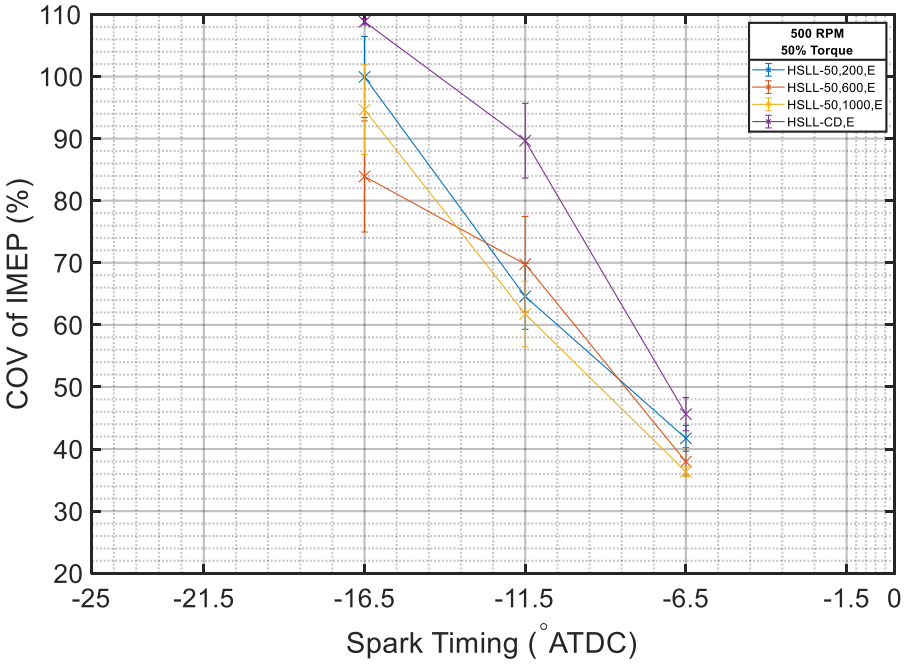

Figure 37: COV of IMEP for 50 mA and varying duration

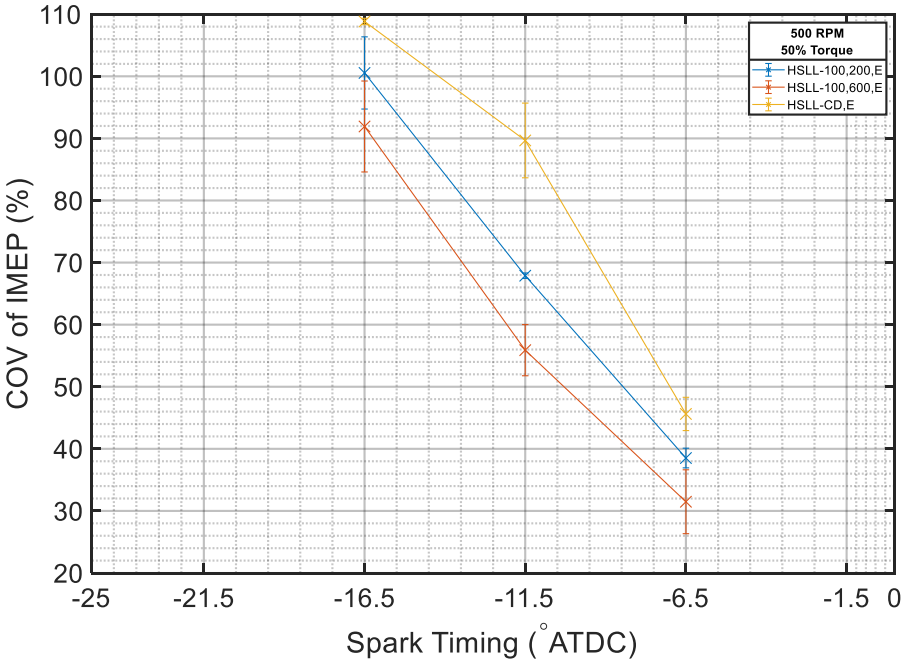

Figure 38: COV of IMEP for 100 mA and varying duration

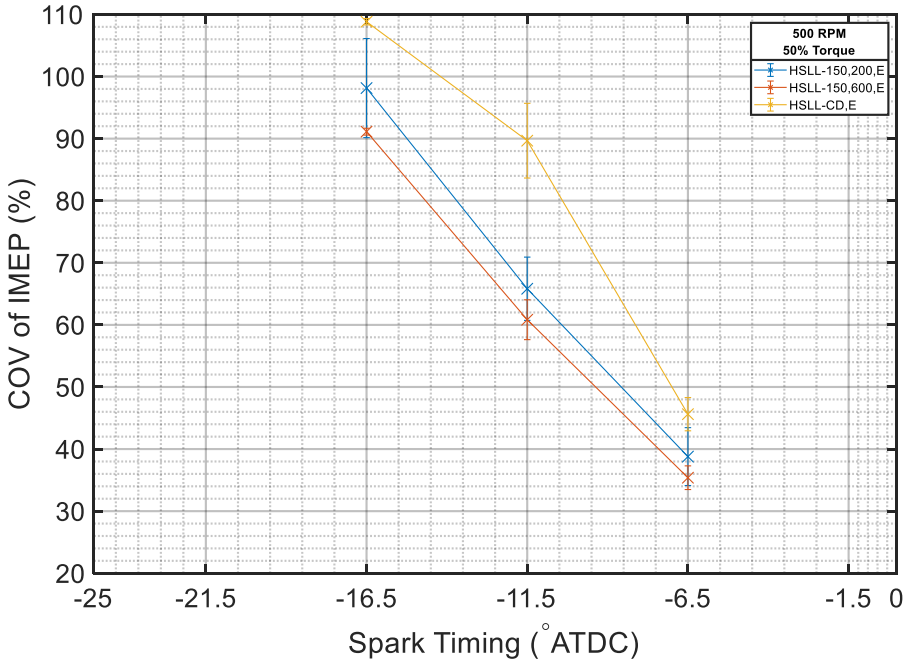

Figure 39: COV of IMEP for 150 mA and varying duration

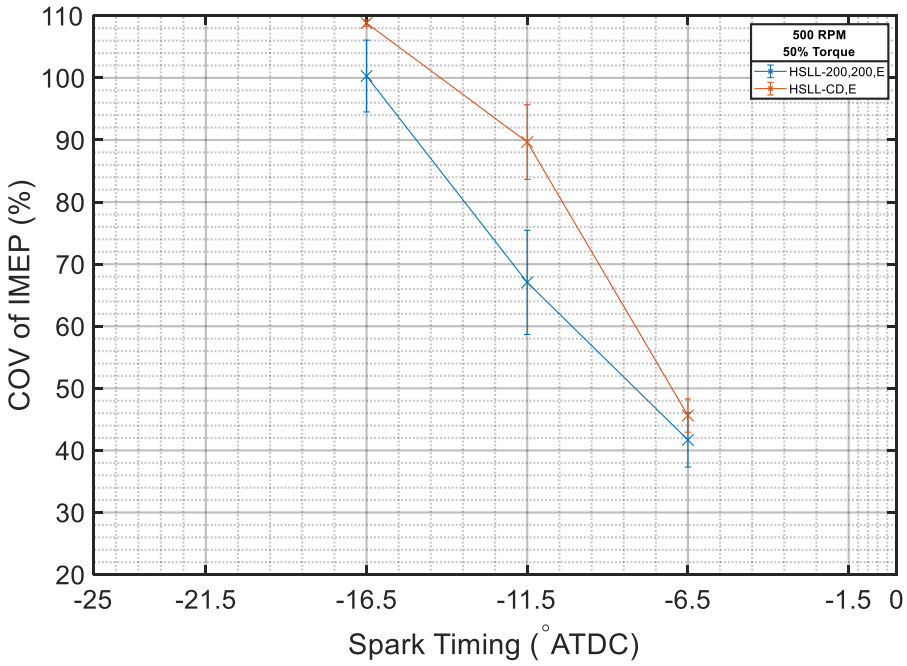

Figure 40: COV of IMEP for 200 mA and varying duration

Comparing the entire range of spark profiles against one another shows no evidence of any trends of spark current or duration, as is also the case with the traditional spark plug. This, again, is due to the overlapping confidence intervals represented by the error bars in the figures. Likewise, the spark profiles that proves to be most optimal for the traditional plug also provide the best stability for the capacitor-embedded plug. At -6.5 CAD ATDC, the 100 mA current and both 200 and 600 µs profiles have the lowest COV of IMEP. At the nominal timing of -11.5 CAD ATDC the spark profile of 150 mA and 200 µs give the most stable engine operation. Then, for the -16.5 CAD ATDC case, the 200 mA and 200 µs profile again result in the most stable operation at that particular spark timing.

The Enerpulse results do not perform as favorably as the traditional spark plug for stability. For the entire sweep of spark timings, the average increase in COV of IMEP using the capacitor-embedded spark plug is 10%. A couple of different factors could be the reasoning for this difference. The most likely influence being the changes in temperature between the testing with the traditional plug and the capacitor-embedded plug. The temperature affects both the fuel and air entering the engine, with the fuel flow rate being much higher during the capacitor spark plug testing campaign. The difference averaged out to 30 ˚F when accounting for changes in temperature throughout each day of testing. Another feasible influence is the location of the spark plug gap in the cylinder. It is unknown how sensitive the engine is to changes in location of the spark plug gap, however any changes in the flow velocity around the gap can have substantial impact on

the initiation of combustion and propagation of the flame front [9, 17]. The other possible explanation is that the capacitor in the Enerpulse spark plug hinders the performance of the directed energy ignition system. If the output from the ignition system is being modified during storage in the capacitor the energy discharge could be changed based upon how quickly the energy is sent across the spark plug gap.

3.2.2. Emissions

This section will be brief in comparison to the traditional spark plug, being as the stability results suggest higher emissions for the latter plug. The spark profiles for the capacitor-embedded plug confirm that at the operating point of 500 RPM and 50% load there are not trends for either spark current or duration. The results will be presented for one current with varying duration with the remaining figures in Appendix A.

3.2.2.1. Nitrogen Oxides

Figure 41 shows the NOx emissions for 50 mA current and varying duration of 200, 600, and 1000 μs.

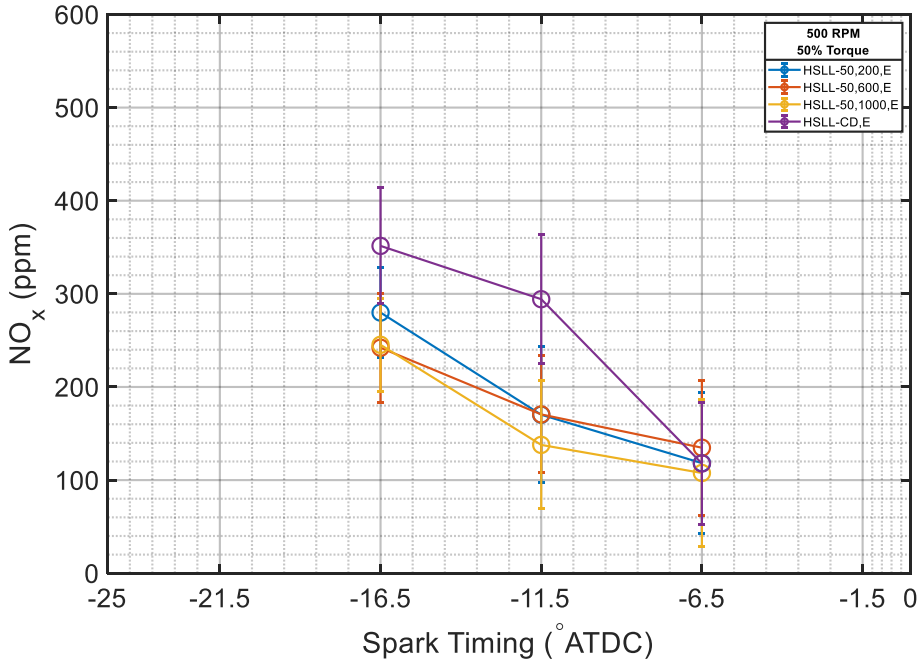

Figure 41: NOx emission for 50 mA and varying duration

As with the traditional spark plug, there is a decrease in emissions of NOx with an increase in stability of the AJAX's performance. No trends are attainable from any of the spark profiles and the results are slightly higher for the Enerpulse plug when compared to the traditional spark plug. The reasoning behind this can be attributed to the previously discussed factors for stability where no statistical significance distinguishes each of the spark profiles. It should also be noted that even though the method of data collection is much more accurate in capturing these emissions, the confidence intervals for this data does not show any improvement over the uncertainty associated with the standard plug data.

3.2.2.2. Total Hydrocarbons

The emissions for unburned THC can be seen below in Figure 42 for the same spark profiles as the NOx figure.

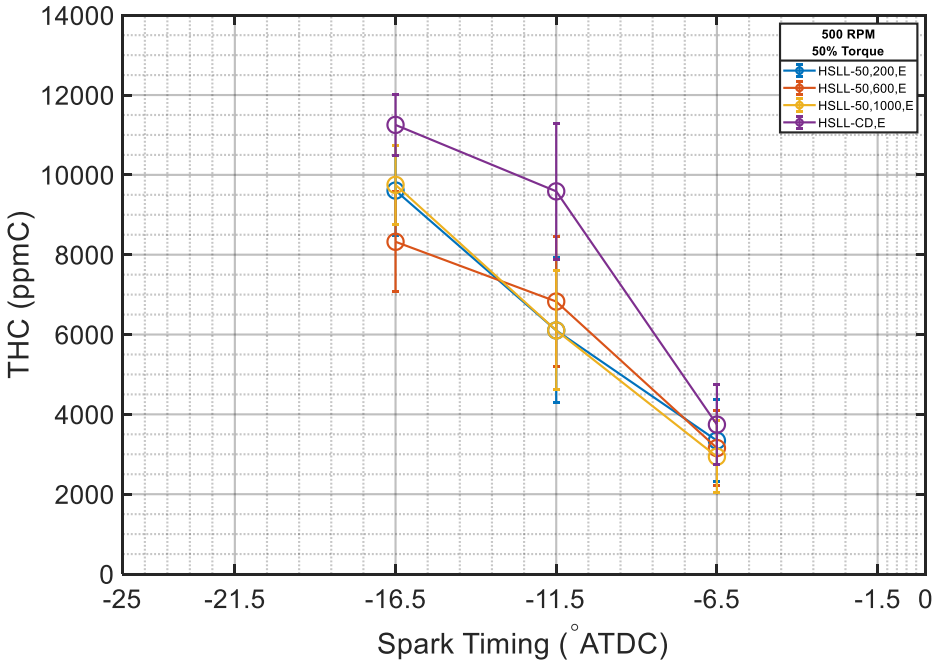

Figure 42: THC emissions for 50 mA and varying duration

Similar to the traditional plug, the capacitor-embedded plug decreases in THC emissions as the combustion becomes more stable, by retarding the spark timing. The general shift in THC is higher than the traditional plug, though the uncertainty is so great that a specific value is not warranted. Once again, not trends are seen in any of the spark profiles for either spark current or duration due to the overlapping confidence intervals.

3.2.2.3. Carbon Monoxide

The CO emission are shown below in Figure 43, for the spark profiles of 50 mA and varying duration.

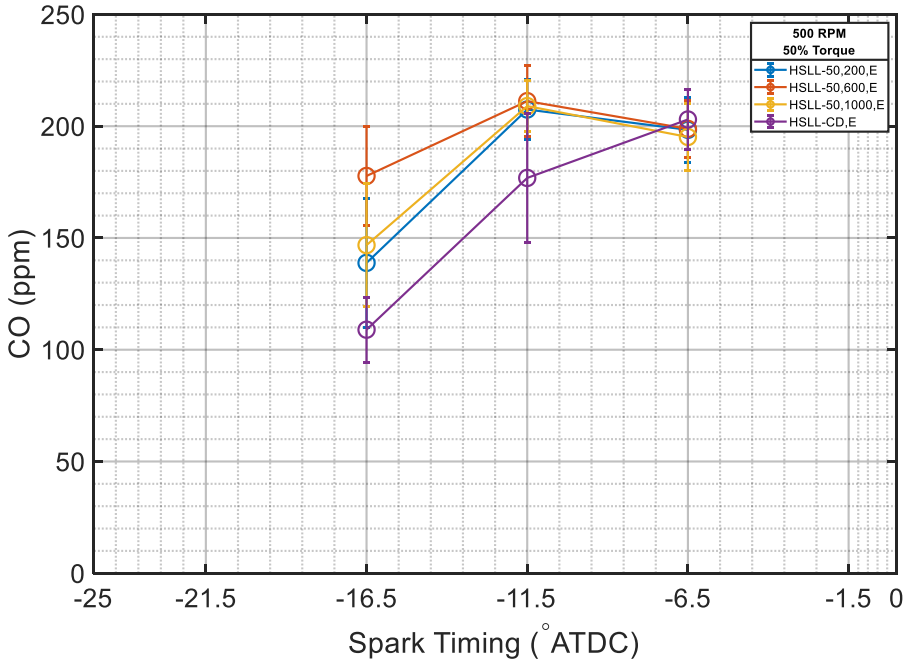

Figure 43: CO emissions for 50 mA and varying duration

Following the trend of the traditional spark plug, the CO emissions increase as the mixture is richened with increasing retard of the spark timing. These emissions, on average, are the same as the traditional spark plug's results though the high level of uncertainty does not allow for a conclusive statement on the matter. As with all emissions beforehand, no distinguishable differences are produced by changing the profile of the spark discharge.

3.2.2.4. Carbon Dioxide

The CO_2 emissions shown below in Figure 44 are for spark profiles of 50 mA current and durations identical to previous results of the capacitor-embedded spark plug.

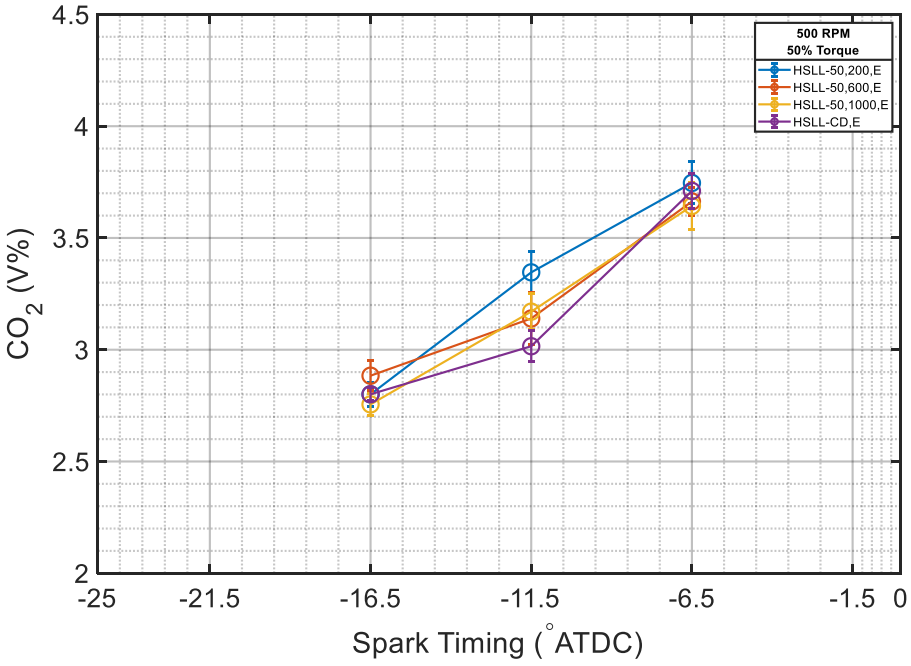

Figure 44: CO_2 emissions for 50 mA and varying duration

The emissions for CO_2 follow the same trend as past findings in increasing in percentage as the mixture is richened towards stoichiometric. The emissions when using the capacitor-embedded plug give about a 0.5% increase in comparison to the traditional spark plug. In addition, no trends are able to be discerned for any of the spark profiles whether it be based on current or duration.

3.2.2.5. Oxygen

Finally, O_2 emissions confirm the validity of the capacitor-embedded results and their relation to the results recorded using the traditional spark plug in the AJAX. Figure 45 displays the O_2 emissions for 50 mA and multiple durations.

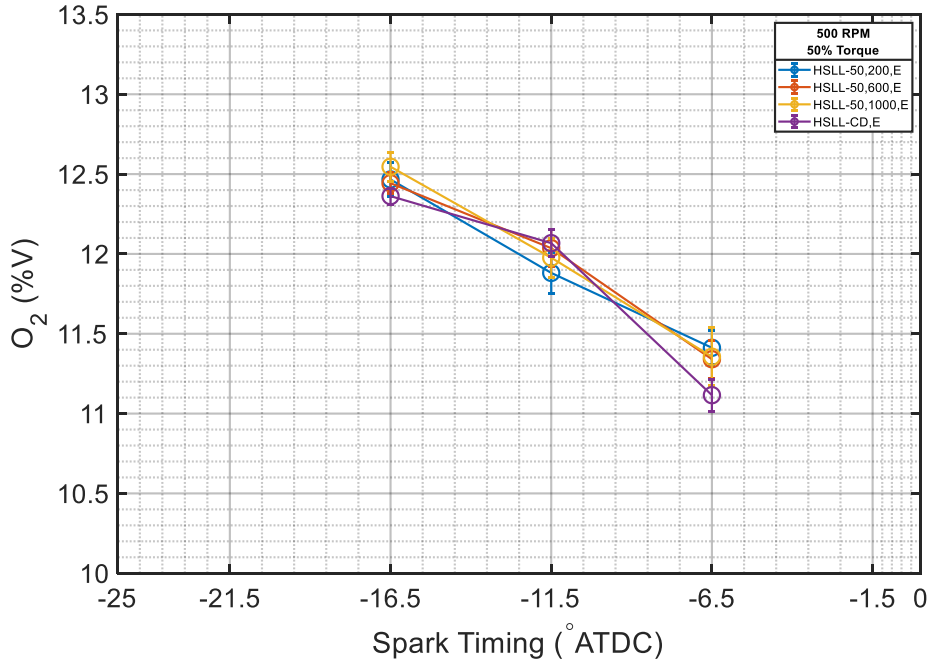

Figure 45: O_2 emissions for 50 mA and varying duration

As expected, the oxygen emissions trend inversely with the CO_2. The overall grouping of the values is a bit lower than the traditional spark plug, which is expected as more fuel is required at this operating point to sustain 500 RPM for half load. Similar to the 0.5% CO_2 increase, a 0.5% O_2 decrease results in using the capacitor-embedded spark plug. No trends are apparent throughout any of the spark profiles, as is expected given the other emissions results and the statistically insignificance of the varying current and duration.

4. CONCLUSIONS

This study assesses the implementation of a directed energy ignition system using a traditional and a capacitor-embedded spark plug on an Ajax E-565 engine for its most fuel-lean operating condition. The goal of the study is to quantify changes in stability and emission performance of the engine by changing the spark current and spark duration sent through the spark plugs.

The traditional spark plug results confirm what has been found before in studies dealing with changes to spark energy discharge. No trends are able to be gathered from the results by varying spark current or duration. There is an improvement of about 20% for engine stability across all spark timings. However, at each spark timing a different spark profile proves most optimal as no profile consistently provides the lowest values of COV of IMEP. Emissions improvements are insignificant as the results show high levels of uncertainty that intertwine with the standard CD baseline. The data collection method used for emissions with the standard spark plug is one of the reasons for the range of uncertainty. The high uncertainty can also be attributed to the specific speed and load used for this study and is consistent with previous research at this engine operating condition.

Using a capacitor-embedded spark plug shows no improvements over the traditional spark plug and, in all cases, performs worse in regards to stability. There are also no indications with this spark plug that any trends exist by changing the spark current or duration. Emissions results show, using the updated means of data collection, that the overlapping 95% confidence intervals render any possible changes that may

come from using the capacitor-embedded plug as statistically insignificant. The poor stability can be linked to a couple of factors, the most likely of which are the cooler temperatures during the test campaign for this plug and the recessed location of the spark plug gap. On an encouraging note, the same spark profiles that prove to be most optimal for each spark timing with the traditional plug are exactly the same for the capacitor-embedded plug.

5. FUTURE WORK

The Ajax E-565 has been a driver of significant research in the Advanced Engine Research Laboratory at Texas A&M University since its installation in 2013. The reliability and simple operation have made for a fantastic means of research for the experienced and novel students alike. Each study continues to build upon the knowledge of past students while providing guidance for future researchers. Following the conclusion of this study, future research opportunities are able to continue what this work has started.

Running the engine at the most fuel-lean condition lead to a relatively unstable operation with large uncertainty in the emissions results. By operating at the most stable condition of high speed and high load, it would be of interest to see if the improvements in stability are similar to those presented in this work. Emissions results should also give lower uncertainty with almost no misfires ever occurring at this operating condition.

If the results of the high speed, high load test show promise of sending more energy through the spark plug, a new ignition system (Altronic CPU-XL) can be installed. This ignition system is able to not only send more energy through the spark plug, but also have more control over when and how much current is discharged throughout the spark event. A study utilizing this system would work well with the use of CFD to optimize the spark profile based upon the flow velocities and AFR around the spark plug gap.

Another technology that has proven to be effective at reducing emissions and improving reliability is the pre-combustion chamber. The chamber uses a small rich

mixture that is ignited by the spark plug. The flame front then expands into the main chamber and ignites the extremely lean mixture present. This technology would provide an excellent study into creating new spark profiles specifically for the pre-chamber to optimize its ability to ignite the rich mixture.

Finally, one of the challenges with the current engine setup is the control and measurement of air flow into the engine. Before installing some sort of compressor to regulate the intake air, a preliminary study can be done on the current air intake system to see how well it does at damping pulsations and giving the ability to collect an accurate air flow reading. The air filter has also been suggested for removal, as the engine is in a lab setting and thus not subjected to the harsh environment of field conditions. Any changes in engine performance of the filter's removal would provide evidence to support the installation of a force-induction device.

REFERENCES

[1] Decision and Information Sciences Division Argonne National Laboratory, "Natural Gas Pipline Technology Overview," 2007.

[2] "Natural gas explained," U.S. Energy Information Administration, 6 December 2019. [Online]. Available: https://www.eia.gov/energyexplained/natural-gas/. [Accessed 11 January 2020].

[3] F. Feijoo, G. C. Iyer, C. Avraam, S. Siddiqui, L. Clarke, S. Sankaranarayanan, M. Binsted, P. Patel, N. Prates, E. Torres-Alfaro and M. Wise, "The future of natural gas infrastructure development in the United States," *Applied Energy,* vol. 228, pp. 149-166, 2018.

[4] N. Newman, "Compressor Stations Doing the Difficult Work," *Pipeline & Gas Journal,* vol. 246, no. 1, 2019.

[5] "Compressor Stations," INGAA, [Online]. Available: https://www.ingaa.org/Pipelines101/Operations/25868.aspx. [Accessed 11 January 2020].

[6] Office of Fossil Energy - U.S. Department of Energy, "How Gas Trubine Power Plants Work," U.S. Department of Energy, [Online]. Available: https://www.energy.gov/fe/how-gas-turbine-power-plants-work. [Accessed 21 January 2020].

[7] S. Mokhatab, W. A. Poe and J. G. Speight, Handbook of Natural Gas Transmission and Processing, Gulf Professional Publishing, 2006.

[8] G. D. Bourn, "Advanced Compressor Engine Controls to Enhance Operation, Reliability and Integrity," Southwest Research Institute, San Antonio, 2004.

[9] J. Heywood, Internal Combustion Engine Fundamentals, New York: McGraw Hill Inc., 1988.

[10] G. Blair, Design and simulation of two-stroke engines, Warrendale: Society of Autmotive Engineers, 1996.

[11] Ajax Iron Works, *Description of Ajax Engines*, Corry: Ajax Iron Works, 1996.

[12] J. B. Heywood and E. Sher, The two-stroke cycle engine: its development, operation, and design, Philadelphia: Taylor & Francis, 1999.

[13] R. Stone, Introduction to Internal Combustion Engines, Warrendale: Society of Automotive Engineers, 1992.

[14] M. Dulger and E. Sher, "Experimental Study on Spark Ignition of Flowing Combustible Mixtures," 2 January 1995. [Online]. Available: https://saemobilus.sae.org/content/951004. [Accessed 22 January 2020].

[15] R. Maly, "Spark Ignition: Its Physics and Effect on the Internal Combustion Engine," *Fuel Economy*, pp. 91-148, 1984.

[16] D. Lepley, S. Zhu, E. Stiropoulou and L. Tozzi, "Optimizing Hihg-Energy Tunable Ignition Technology: Preventing Electrode Damage whiel Extending the Lean

Flammability Limit of Gas Engines," in *Gas Machinery Conference*, Nashville, 2014.

[17] J. Lepley, D. Lepley and D. Bell, "Validation and Performance Analysis of a Directed Energy Ignition System on Large Natural Gas-Fueled Reciprocating Engines," in *Gas Machinery Conference*, 2011.

[18] J. Lepley, D. Lepley, D. Bell and M. Porter, "Field Validation of a Directed Energy Ignition System on Large Bore Natural Gas-Fueled Reciprocating Engines," in *Gas Machinery Conference*, 2012.

[19] C. R. Stone and A. B. Steele, "Measurement and Modeling of Ignition System Energy and its Effect on Engine Performance," *Proceedings of the Institution of Mechanical Engineers, Part D: Journal of Automobile Engineering*, vol. 203, no. 4, pp. 277-286, 1989.

[20] Ajax Iron Works, *Economical and Dependable Ajax Gas Engine and Oil Engine*, Corry: Ajax Iron Works.

[21] Altronic LLC., *Installation and Operating Manual NGI-1000 Digital Ignition System,* 2017.

[22] Taylor Dynamometer, *DEA150 Air-Cooled Eddy Current Dynamometer.*

[23] Cambustion Ltd., "Operating Principles," [Online]. Available: https://www.cambustion.com/products/ndir500/operating-principle. [Accessed 15 January 2020].

[24] Cambustion Ltd., "CLD Principles," [Online]. Available: https://www.cambustion.com/products/cld500/cld-principles. [Accessed 15 January 2020].

[25] Cambustion Ltd., "Fast FID Principles," [Online]. Available: https://www.cambustion.com/products/hfr500/fast-fid-principles. [Accessed 15 January 2020].

[26] Horiba Ltd., *MEXA-7000 MCU Operation Instruction Manual,* 2007.

[27] L. J. Kastner, "An Investigation of the Airbox Method of Measuring the Air Consumption of Internal Combustion Engines," vol. 157, no. 1, pp. 387-404, 1947.

[28] A. Karvountzis-Kontakiotis, L. Ntziachristos, Z. Samaras, A. Dimaratos and M. Peckham, "Experimental Investigation of Cyclic Variability on Combustion and Emissions of a High-Speed SI Engine," Society of Automotive Engineers International, 2015.

[29] J. Brown, *Implementable Changes to a Large-Bore Singl Cylinder Natural Gas Engine for Improved Emissions Performance,* 2017.

[30] G. Beshouri, "Characterization and Detection of Typical Combustion Aberrations," Hoerbiger.

[31] A. Griffin, *Combustion Characteristics of a Two-Stroke Large Bore Natural Gas Spark-Ignited Engine,* College Station, 2015.

[32] A. M. Helmenstine, "1," ThoughCo., 14 January 2020. [Online]. Available: https://www.thoughtco.com/carbon-monoxide-poisoning-4048941. [Accessed 17 January 2020].

[33] ATMOS Energy-Mid-Tex/APT, "Chromatograph Report," College Station, 2019.

[34] Horiba Ltd., *CO/CO2 Analyzer AIA-72X Series*, Kyoto, 2007.

[35] Horiba Ltd., *NO/NOx Analyzer CLA-720MA*, 2007.

[36] Horiba Ltd., *O2 Analyzer MPA-720*, 2007.

[37] Horiba Ltd., *THC Analyzer FIA-725A*, 2007.

[38] A. Bajwa, *First and Second Law Analyses of a Large Bore Two Storke Spark Ignition Engine Fueled with Natural Gas*, College Station, 2016.

APPENDIX A- ALTERNATIVE RESULT FIGURES

The figures show below are of the same data presented in the results. Here, the current is varied in each figure while the duration is held constant. The data is presented in the same order as the results as well.

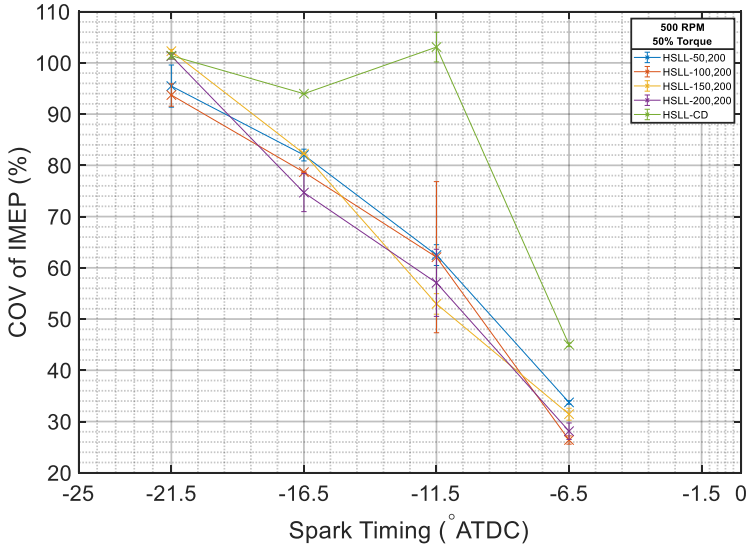

Figure 46: COV of IMEP for 200 µs and varying current

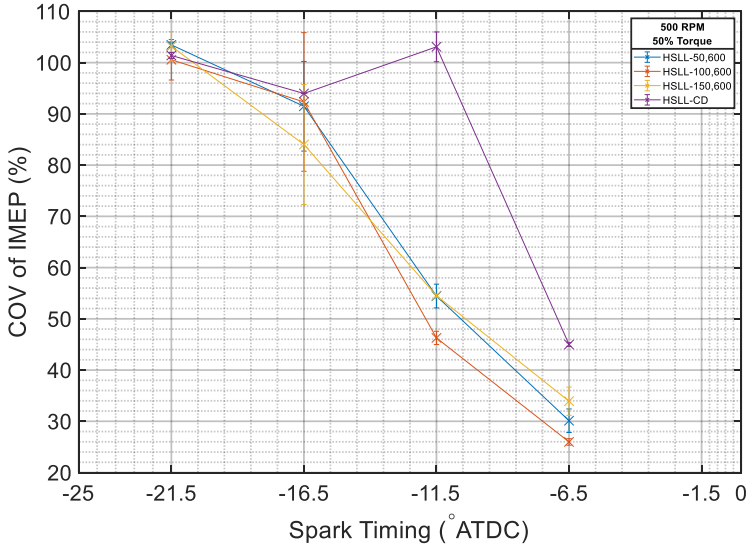

Figure 47: COV of IMEP for 600 µs and varying current

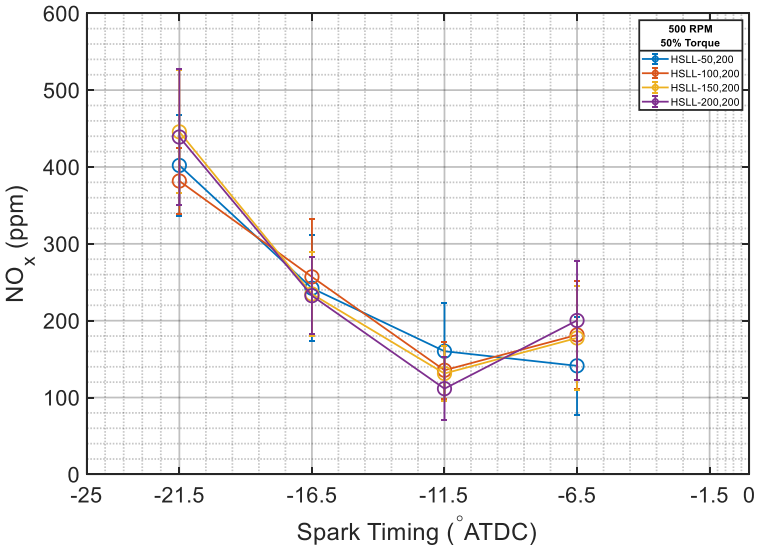

Figure 48: NOx emissions for 200 µs and varying current

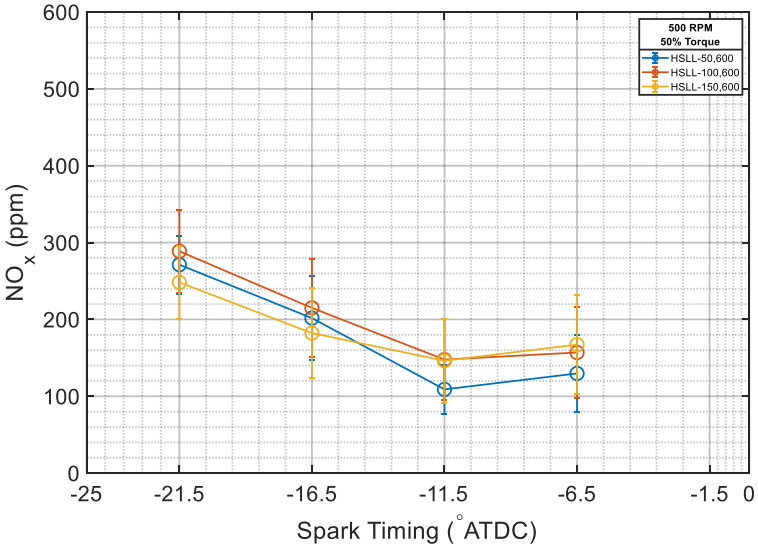

Figure 49: NOx emissions for 600 µs and varying current

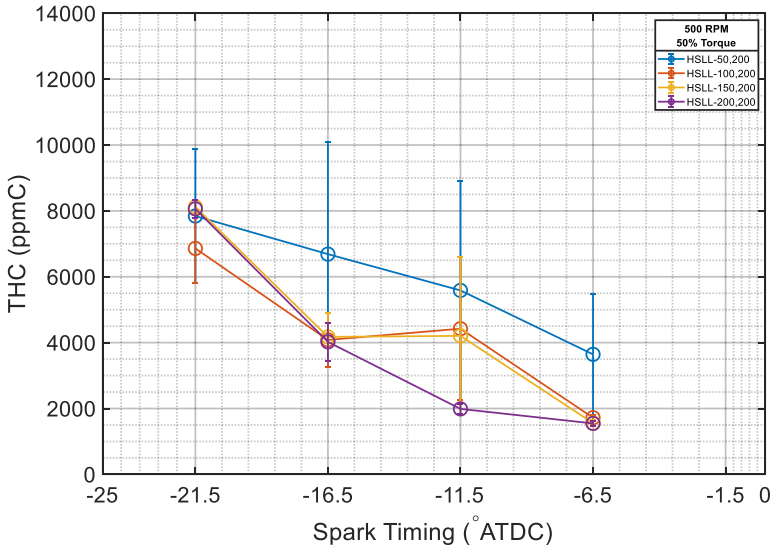

Figure 50: THC emissions for 200 µs and varying current

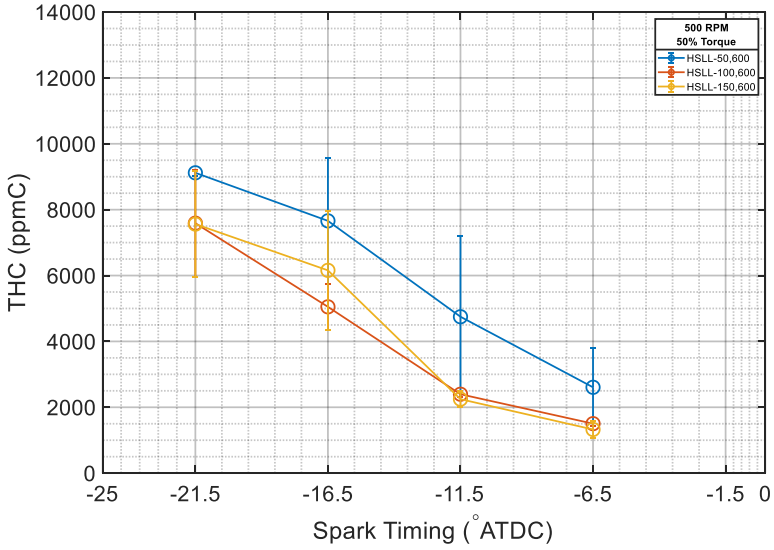

Figure 51: THC emissions for 600 µs and varying current

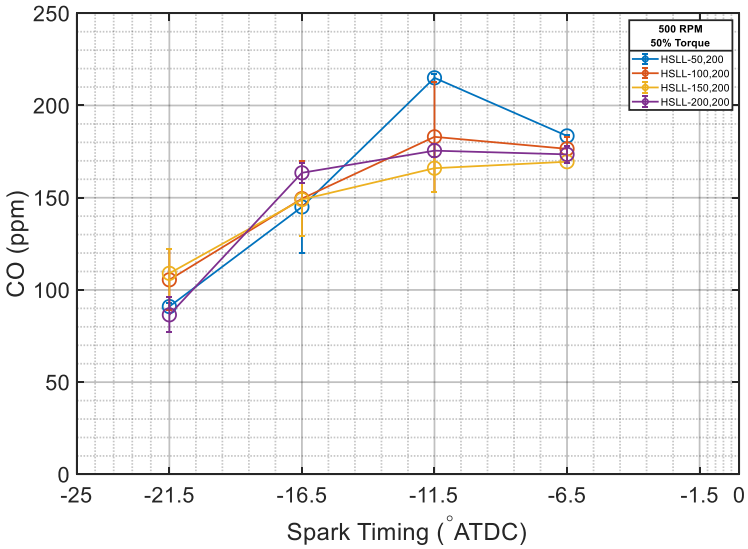

Figure 52: CO emissions for 200 µs and varying current

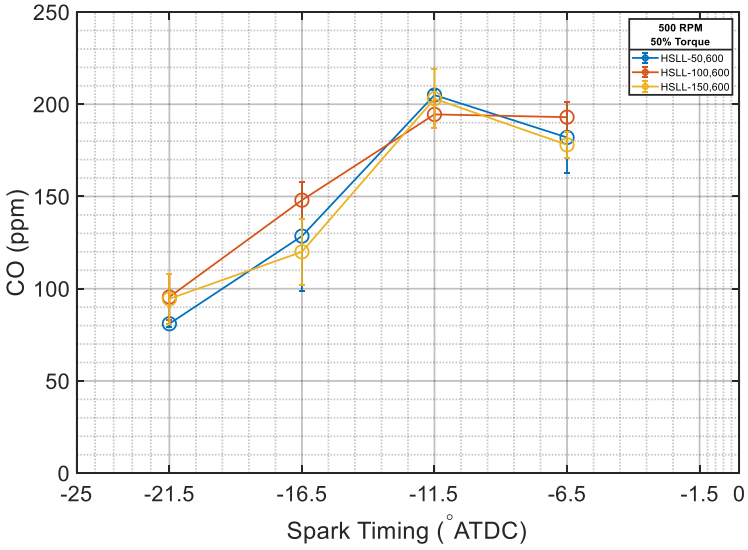

Figure 53: CO emissions for 600 µs and varying current

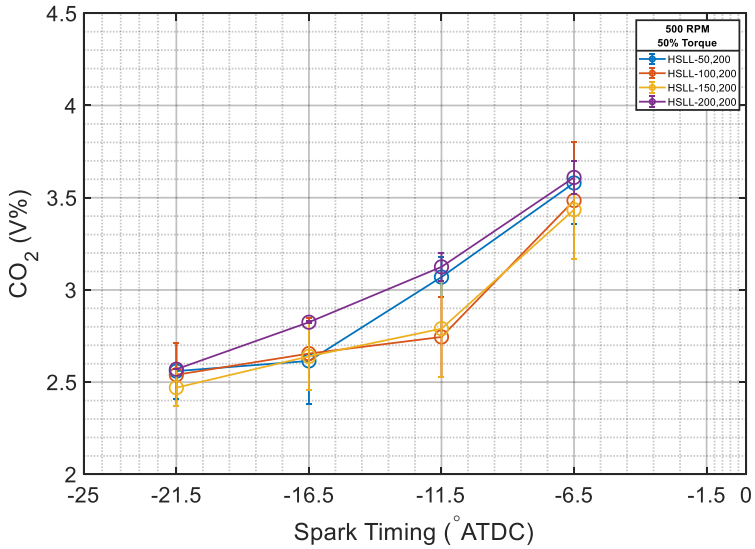

Figure 54: CO_2 emissions for 200 µs and varying current

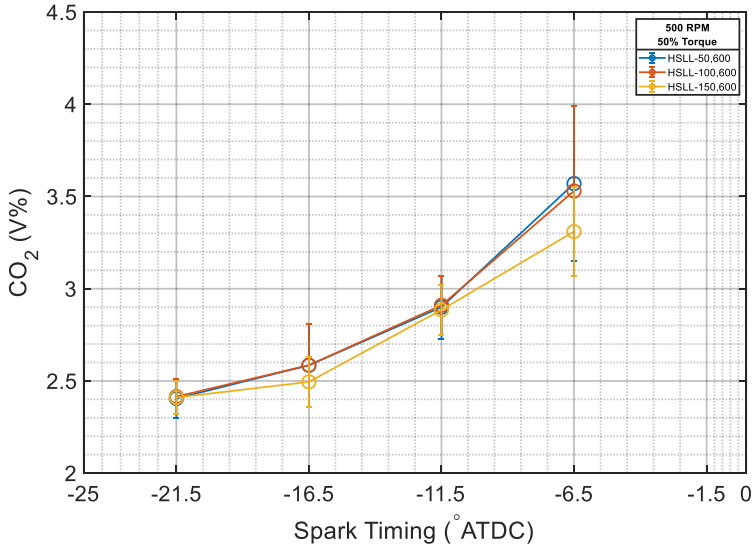

Figure 55: CO_2 emissions for 600 µs and varying current

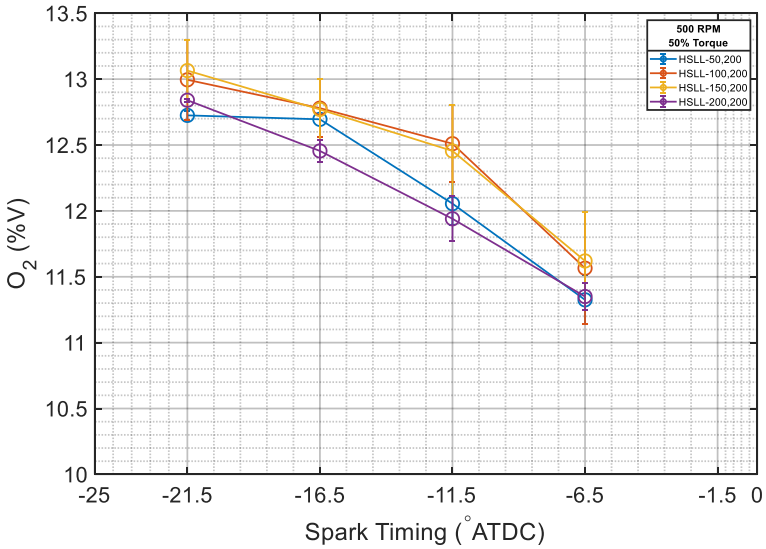

Figure 56: O_2 emissions for 200 µs and varying current

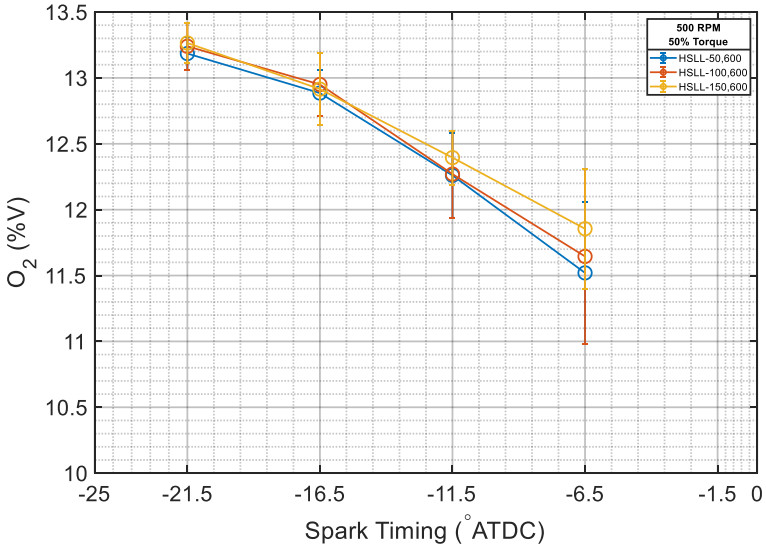

Figure 57: O_2 emissions for 600 µs and varying current

APPENDIX B- NATURAL GAS COMPOSITION

The report below is a readout of the natural gas composition for the Advanced Engine Research Lab during the month of October 2019.

Effective Date	Sat. HV	As Del HV	Dry HV	Meas. HV	Water Content	Wobbe	Real Gravity	C1	C2	C3	IC4	NC4	IC5	NC5	C6	C7	C8	C9	C10	N2	CO2
10/01/2019 09:00	985.3	0.0	1002.8	0.0		1316.1	0.5805	95.2875	2.1000	0.1305	0.0074	0.0156	0.0031	0.0029	0.0004	0.0004	0.0000	0.0000	0.0000	1.7975	0.6547
10/02/2019 09:00	984.5	0.0	1002.0	0.0		1314.8	0.5808	95.2837	2.0674	0.1256	0.0078	0.0154	0.0031	0.0027	0.0004	0.0004	0.0000	0.0000	0.0000	1.7873	0.7062
10/03/2019 09:00	986.4	0.0	1004.0	0.0		1315.1	0.5829	94.8566	2.3920	0.1596	0.0062	0.0111	0.0019	0.0017	0.0000	0.0000	0.0000	0.0000	0.0000	1.8652	0.7057
10/04/2019 09:00	984.8	0.0	1002.3	0.0		1313.9	0.5819	95.0047	2.2381	0.1328	0.0070	0.0146	0.0027	0.0024	0.0003	0.0003	0.0000	0.0000	0.0000	1.9229	0.6741
10/05/2019 09:00	986.8	0.0	1004.4	0.0		1316.6	0.5820	94.9976	2.3165	0.1470	0.0091	0.0196	0.0039	0.0036	0.0008	0.0008	0.0000	0.0000	0.0000	1.8702	0.6308
10/06/2019 09:00	985.7	0.0	1003.2	0.0		1315.3	0.5817	95.0052	2.2318	0.1506	0.0094	0.0215	0.0043	0.0040	0.0010	0.0010	0.0000	0.0000	0.0000	1.9748	0.5966
10/07/2019 09:00	984.4	0.0	1001.9	0.0		1313.9	0.5814	95.0831	2.1521	0.1430	0.0073	0.0152	0.0028	0.0026	0.0007	0.0007	0.0000	0.0000	0.0000	1.9474	0.6451
10/08/2019 09:00	983.8	0.0	1001.3	0.0		1313.4	0.5812	95.1640	2.0673	0.1372	0.0084	0.0173	0.0035	0.0032	0.0011	0.0011	0.0000	0.0000	0.0000	1.9257	0.6712
10/09/2019 09:00	983.6	0.0	1001.1	0.0		1315.0	0.5796	95.4362	1.9671	0.1085	0.0059	0.0118	0.0024	0.0021	0.0001	0.0001	0.0000	0.0000	0.0000	1.8113	0.6544
10/10/2019 09:00	986.1	0.0	1003.7	0.0		1317.1	0.5808	95.0953	2.2856	0.1234	0.0058	0.0122	0.0023	0.0020	0.0003	0.0003	0.0000	0.0000	0.0000	1.9235	0.5492
10/11/2019 09:00	983.6	0.0	1001.1	0.0		1314.0	0.5805	95.1454	2.1570	0.1003	0.0042	0.0078	0.0013	0.0012	0.0003	0.0003	0.0000	0.0000	0.0000	1.9899	0.5924
10/12/2019 09:00	984.1	0.0	1001.6	0.0		1315.6	0.5796	95.2753	2.0539	0.1184	0.0067	0.0152	0.0031	0.0030	0.0011	0.0011	0.0000	0.0000	0.0000	2.0228	0.4993
10/13/2019 09:00	982.1	0.0	999.6	0.0		1313.7	0.5790	95.4145	1.9437	0.0854	0.0036	0.0070	0.0013	0.0011	0.0002	0.0002	0.0000	0.0000	0.0000	1.9754	0.5677
10/14/2019 09:00	983.0	0.0	1000.5	0.0		1314.4	0.5794	95.3319	2.0010	0.1022	0.0052	0.0113	0.0022	0.0021	0.0002	0.0002	0.0000	0.0000	0.0000	1.9964	0.5473
10/15/2019 09:00	984.2	0.0	1001.7	0.0		1316.9	0.5786	95.4317	2.0143	0.1045	0.0053	0.0109	0.0020	0.0019	0.0000	0.0000	0.0000	0.0000	0.0000	1.9542	0.4752
10/16/2019 09:00	984.6	0.0	1002.1	0.0		1317.0	0.5790	95.2376	2.1381	0.1144	0.0045	0.0098	0.0016	0.0015	0.0003	0.0003	0.0000	0.0000	0.0000	2.1205	0.3715
10/17/2019 09:00	983.4	0.0	1000.9	0.0		1314.0	0.5802	95.1568	2.1103	0.1159	0.0056	0.0088	0.0016	0.0013	0.0003	0.0003	0.0000	0.0000	0.0000	2.0561	0.5430
10/18/2019 09:00	982.1	0.0	999.6	0.0		1312.4	0.5801	95.2798	2.0120	0.0978	0.0032	0.0057	0.0005	0.0002	0.0000	0.0000	0.0000	0.0000	0.0000	1.9406	0.6603
10/19/2019 09:00	983.6	0.0	1001.1	0.0		1314.3	0.5802	95.2684	2.0919	0.0983	0.0039	0.0075	0.0012	0.0008	0.0000	0.0000	0.0000	0.0000	0.0000	1.8745	0.6534
10/20/2019 09:00	982.0	0.0	999.5	0.0		1312.6	0.5798	95.3212	2.0268	0.0721	0.0024	0.0036	0.0003	0.0001	0.0000	0.0000	0.0000	0.0000	0.0000	1.9078	0.6657
10/21/2019 09:00	982.2	0.0	999.7	0.0		1312.5	0.5801	95.2586	2.0477	0.0853	0.0033	0.0045	0.0007	0.0003	0.0001	0.0001	0.0000	0.0000	0.0000	1.9384	0.6610
10/22/2019 09:00	983.2	0.0	1000.7	0.0		1313.9	0.5801	95.2472	2.1020	0.0903	0.0035	0.0052	0.0009	0.0006	0.0000	0.0000	0.0000	0.0000	0.0000	1.9228	0.6274
10/23/2019 09:00	983.2	0.0	1000.7	0.0		1313.9	0.5801	95.2472	2.1020	0.0903	0.0035	0.0052	0.0009	0.0006	0.0000	0.0000	0.0000	0.0000	0.0000	1.9228	0.6274
10/24/2019 09:00	983.2	0.0	1000.7	0.0		1313.9	0.5801	95.2472	2.1020	0.0903	0.0035	0.0052	0.0009	0.0006	0.0000	0.0000	0.0000	0.0000	0.0000	1.9228	0.6274
Flow Weighted Averaae:	984.0	0.0	1001.5	0.0			0.5804	95.2078	2.1168	0.1139	0.0055	0.0109	0.0020	0.0018	0.0003	0.0003	0.0000	0.0000	0.0000	1.9378	0.6029

Figure 58: Natural Gas composition in AERL lab during test campaign [33]

APPENDIX C-INSTRUMENTATION

The figures below describe the specifications for the MEXA 7100-D and each of its individual analyzers. These include the CO/CO_2, NO/NOx, O_2, and THC analyzers that had data presented in the results. The uncertainty related to each of the analyzers is minimal in comparison the variance that is observed in repeated tests for each spark profile.

● **Function and performance*2**

Response (T_{90})	AIA-721 series: Within 2.0 s (at the flow rate of 3 L/min from ANR CAL-IN inlet) AIA-722, 723 series: Within 1.5 s (at the flow rate of 2 L/min from ANR CAL-IN inlet)
Noise	Peak-to-Peak of total 5 minutes of duration less than 1.0% of the full scale
Linearity	Within ±1.0% of the full scale or ±2.0% of the readings, whichever is small
Repeatability	Within ±0.5% of the full scale for zero point, or within ±0.5% of the readings for span point
Drift	Within ±1.0% of the full scale/24 h for zero point, Within ±1.0% of the readings/24 h for span point (temperature variation within ±2°C)

Figure 59: CO/CO_2 analyzer uncertainty [34]

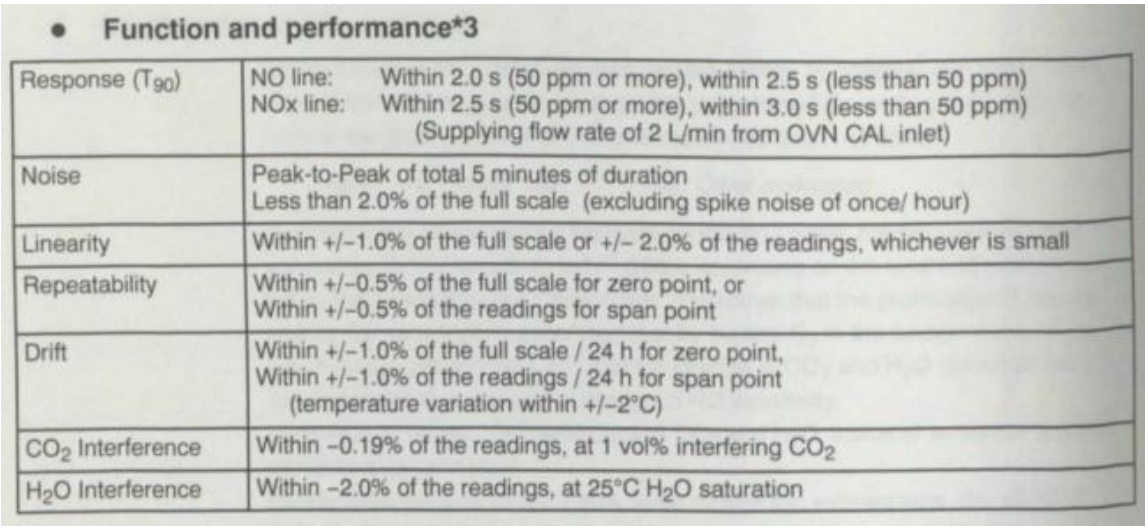

- **Function and performance*3**

Response (T_{90})	NO line: Within 2.0 s (50 ppm or more), within 2.5 s (less than 50 ppm) NOx line: Within 2.5 s (50 ppm or more), within 3.0 s (less than 50 ppm) (Supplying flow rate of 2 L/min from OVN CAL inlet)
Noise	Peak-to-Peak of total 5 minutes of duration Less than 2.0% of the full scale (excluding spike noise of once/ hour)
Linearity	Within +/−1.0% of the full scale or +/− 2.0% of the readings, whichever is small
Repeatability	Within +/−0.5% of the full scale for zero point, or Within +/−0.5% of the readings for span point
Drift	Within +/−1.0% of the full scale / 24 h for zero point, Within +/−1.0% of the readings / 24 h for span point (temperature variation within +/−2°C)
CO_2 Interference	Within −0.19% of the readings, at 1 vol% interfering CO_2
H_2O Interference	Within −2.0% of the readings, at 25°C H_2O saturation

Figure 60: NO/NOx analyzer uncertainty [35]

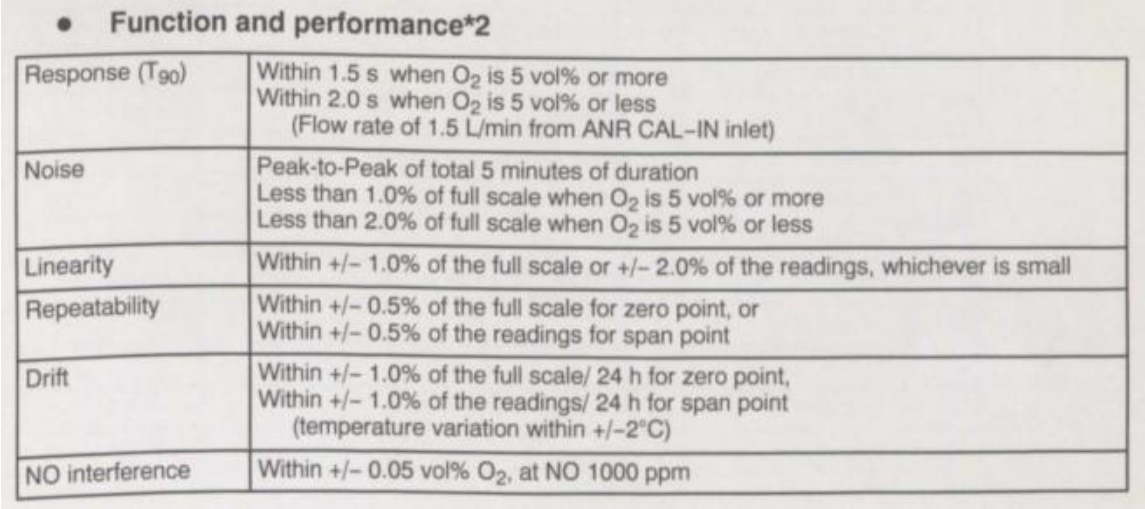

- **Function and performance*2**

Response (T_{90})	Within 1.5 s when O_2 is 5 vol% or more Within 2.0 s when O_2 is 5 vol% or less (Flow rate of 1.5 L/min from ANR CAL−IN inlet)
Noise	Peak-to-Peak of total 5 minutes of duration Less than 1.0% of full scale when O_2 is 5 vol% or more Less than 2.0% of full scale when O_2 is 5 vol% or less
Linearity	Within +/− 1.0% of the full scale or +/− 2.0% of the readings, whichever is small
Repeatability	Within +/− 0.5% of the full scale for zero point, or Within +/− 0.5% of the readings for span point
Drift	Within +/− 1.0% of the full scale/ 24 h for zero point, Within +/− 1.0% of the readings/ 24 h for span point (temperature variation within +/−2°C)
NO interference	Within +/− 0.05 vol% O_2, at NO 1000 ppm

Figure 61: O_2 analyzer uncertainty [36]

- **Function and performance *2**

Response (T_{90})	Within 1.5 s (Flow rate of 2.0 L/min from OVN CAL–IN inlet)
Noise	Peak-to-Peak of total 5 minutes of duration Less than 1.0 % of the full scale
Linearity	Within ±1.0% of the full scale or within ±2.0% of the readings, whichever is small
Repeatability	Within ±0.5% of the full scale for zero point, or Within ±0.5% of the readings for span point
Drift	Within ±1.0% of the full scale/ 24 h for zero point, Within ±1.0% of the readings/ 24 h for span point (temperature variation within ±2°C)
O_2 interference	Within ±2.0% of the readings for C_3H_8 375 ppmC ±50 ppmC, at 0 vol% to 21 vol% O_2

Figure 62: THC analyzer uncertainty [37]

APPENDIX D- UNCERTAINTY CALCULATIONS

Emissions uncertainty was calculated using two different methods during this study. The portion of the study using the traditional spark plug only collected a minimum and maximum value. The computer was then upgraded soon after to have the capability to collect data throughout a set length of time, thus giving hundreds of values to work with for the capacitor-embedded spark plug test campaign.

Traditional Spark Plug

A maximum and minimum value is recorded for each emission constituent over a period of 30 seconds. An average of the values is then calculated.

$$\bar{x} = \frac{x_{max} + x_{min}}{2}$$

A simple uncertainty calculation is made using the mean and the maximum value. This gives the range of the error bars.

$$Uncertainty = x_{max} - \bar{x}$$

Thus, giving the following that is seen on all of the figures for emissions of the traditional spark plug.

At each spark timing: $\bar{x} \pm Uncertainty$

Capacitor-Embedded Spark Plug

Since more data is now able to be collected with the computer upgrades a more traditional uncertainty calculation is used. The calculations used below are identical of those used in other emissions studies for the Ajax E-565 [29, 31].

$$Uncertainty = z^* \cdot \frac{\sigma}{\sqrt{n}}$$

Here, $z^*$is the level of confidence, σ is the standard deviation, and n is the sample size used to compute the uncertainty. Using a 95% confidence interval gives

$$z^* = 1.96$$

Thus, the following is used on all figures for emissions of the capacitor-embedded spark plug.

$$\text{At each spark timing: } \bar{x} \pm 1.96 \cdot \frac{\sigma}{\sqrt{n}}$$

Stability

The stability calculations for both spark plugs used an identical uncertainty calculation to the capacitor-embedded spark plug.

APPENDIX E- ATMOSPHERIC CONDITIONS FOR TESTING

The lab conditions are nearly identical to the outside conditions at Texas A&M on any given day of testing. As such, as the weather changes during the fall season, it was impossible to control the temperature during the second half of the testing campaign for this study. Table 4 gives the average temperature conditions during each day's testing. All tests were conducted during afternoon hours so as to reduce the impact of temperature changes in the mornings and evenings.

Table 4: Testing conditions during study

Test	Temperature (ºF)	Pressure (in. Hg)
Traditional Spark Plug, Round 1	98	30.08
Traditional Spark Plug, Round 2	95	29.65
Capacitor Spark Plug, Round 1	58	29.96
Capacitor Spark Plug, Round 2	64	29.83